Ability of a SVAT and a two-source energy balance model to predict evapotranspiration for several crops and climate conditions

G. Bigeard[1,2], B. Coudert[1,2], J. Chirouze[1], S. Er-Raki[3], G. Boulet[1,4], E. Ceschia[1,2], and L. Jarlan[1,3]

[1]CESBIO, Toulouse, France
[2]Université Paul Sabatier, Toulouse, France
[3]Université Cadi Ayyad, Marrakech, Morocco
[4]IRD, Institut National Agronomique de Tunisie, Tunis, Tunisia

Correspondence: B. Coudert (benoit.coudert@cesbio.cnes.fr)

Abstract. Agrosystems heterogeneity, in terms of hydric conditions, crop types and states, and meteorological forcing, is difficult to characterize precisely at the field scale over an agricultural landscape. This study aims to perform a sensitivity study to uncertain model inputs of two classical approaches used to map evapotranspiration of agrosystems: (1) a Surface Energy Balance (SEB) model, the Two Source Energy Balance (TSEB), forced with TIR data as a proxy of the crop hydric conditions, and (2) a Soil-Vegetation-Atmosphere Transfer (SVAT) model, the SEtHyS model, where hydric conditions are computed from a soil water budget. To this objective, models skills are compared thanks to a large and unique *in situ* database covering different crops and climate conditions, acquired over three experimental sites in southern France and Morocco. On average, models provide half-hourly estimations of latent heat flux (LE) with a RMSE of around 55 Wm^{-2} for TSEB and 47 Wm^{-2} for SEtHyS, and estimations of sensible heat flux (H) with a RMSE of around 29 Wm^{-2} for TSEB and 38 Wm^{-2} for SEtHyS. A sensitivity analysis based on realistic errors aimed to estimate the potential loss of performance induced by spatialization process. For the SVAT model, the MCIP methodology is used to determine and test different sets of parameters. TSEB is run with only one set of parameters and provides acceptable performances for all crop stages apart from the early beginning of the growing season (LAI < 0.2 m^2 m^{-2}) and when water stress occurred. An in-depth study on the Priestley-Taylor key parameter highlights its marked diurnal cycle and the need to adjust its value to improve flux partition between sensible and latent heat fluxes (1.5 and 1.25 for France and Morocco, respectively). Optimal values of 1.8 to 2 were highlighted under cloudy conditions, which is of particular interest with the emergence of low altitude drone acquisition. Under developed vegetation (LAI > 0.8 m^2 m^{-2}) and unstressed conditions, using sets of parameters that only differentiate crop types is a valuable tradeoff for SEtHyS. This study provides some scientific elements for a joint use of both approaches and TIR imagery, via the development of new data assimilation and calibration strategies.

1 Introduction

Exchange of water at the soil-vegetation-atmosphere interface is of prime importance for weather forecasting and for climate studies (Shukla and Mintz, 1982); it is also a key component for hydrology, and therefore catchment water balance (Milly, 1994), and for agronomy in order to improve irrigation scheduling (Allen et al., 1998). Despite the abundant literature on the

subject, there is no consensual approach for its spatialized estimation, and the contribution of evapotranspiration (ET) to the global hydrologic cycle remains uncertain (Jasechko et al., 2013). There are several *in situ* techniques available to measure ET (Allen et al., 2011) but most suffer from a lack of spatial representativeness. This prevents their use as a sustainable solution for regional applications, especially for agricultural landscape where spatial heterogeneity –in terms of farming and technical itineraries including the resulting pattern of moisture conditions– is high. By contrast, remote sensing offers an attractive alternative through the synoptic and repeated data acquisition it provides. Indeed, even if ET is not directly observable from space, remote sensing data in different parts of the electromagnetic spectrum are related to the characteristics of the land surface governing the evapotranspiration process.

Within this context, several approaches combining remote sensing data and land surface models of various complexity were proposed for the regional monitoring of ET (Courault et al., 2005), from the most conceptual approaches modulating the evaporative demand by an empirical coefficient (the so called "crop coefficient", Allen et al., 1998), to the complex and mechanistically-based Soil-Vegetation-Atmosphere Transfer (SVAT) models that require a large number of inputs. In-between, the surface energy balance (SEB) models, constrained by thermal-infrared radiative temperature observations, have been gaining influence over the last decade (Choi et al., 2009; Diarra et al., 2017). Several authors intercompared the different SEB-based approaches for mapping ET with noticeable discrepancies (see Zhan et al., 1996; French et al., 2005; Timmermans et al., 2007, 2011; Chirouze et al., 2014). Among the different SEB models, the two-source-energy balance (TSEB Norman et al., 1995) emerged as a robust and accurate model for evapotranspiration mapping over semi-arid crops (Anderson et al., 2007; Chirouze et al., 2014; Diarra et al., 2017). This model is now extensively used in the scientific community and has been the subject of numerous refinements since the original version of Norman (Kustas and Norman, 1999, 2000; Anderson et al., 2008; Colaizzi et al., 2012, 2014, etc...). Nevertheless, both approaches were rarely compared while the joint use, through data assimilation technics, of snapshot evapotranspiration maps from SEB approaches and dynamic SVAT predictions appears promising (Crow et al., 2005, 2008). This is certainly to be attributed to the different underlying diagnostic or prognostic equations of the models with respect to the distinct purposes of the approaches in terms of temporal and/or spatial resolutions of evapotranspiration estimates.

Either based on SVAT or SEB models, the estimation of surface evapotranspiration implies dealing with the method-model complexity issue (Carlson, 2007; Kalma et al., 2008), and with the always incomplete knowledge to document or to constrain them. For instance, with regards to remotely sensed TIR data, McCabe and Wood (2006) have shown how spatial resolution of TIR data used as input in SEB method impacted the spatial variation of flux estimates. For the higher resolution, another source of uncertainty is coming from to the surface temperature fluctuations in relation with atmospheric turbulence (Lagouarde et al., 2013). The lack of knowledge on scaling effects when fluxes are intercompared at the same scales using aggregation or disaggregation methods was also pointed out by several authors as a scientific issue for evapotranspiration mapping (Kustas et al., 2003, 2004; Norman et al., 2003). Although limited in time and focused on semi-arid and sparse grasses and crops, several studies were also dedicated to the sensitivity analysis of the TSEB model to uncertain inputs including radiative temperature, meteorological forcings or vegetation descriptors (Zhan et al., 1996; Anderson et al., 1997; Kustas and Norman, 1997; Li and Kustas, 2005; Timmermans et al., 2007; Kustas et al., 2012). Likewise, others were focused on the sensitivity of SVATs (Franks

et al., 1997; Calvet et al., 1998; Wood et al., 1998; Pitman et al., 1999; Olioso et al., 1999; Robock et al., 2003; Petropoulos et al., 2009). Within this context, the comparative study of Crow et al. (2008) between a SVAT model and the TSEB approach is a founding study of our work. Indeed, as a preliminary step to the joint use of both approaches through data assimilation, the purpose of this study is the comparison of the TSEB model (Norman et al., 1995) and the SEtHyS SVAT model (described in Coudert et al., 2006), in terms of overall performances, errors and domains of validity when model inputs and parameters are uncertain. This is done here thanks to large and unique in situ database covering several crops and seasons in relatively well-watered conditions and limited advection environment.

This paper is organized as follows. After briefly introducing data sets and both models (Sect. 2), the analysis of the models performances is presented (Sect. 3.1). Then, we focus on sensitivity analysis results (Sect. 3.2) and on discussions related to parameters and inputs (Sect. 4). Finally, conclusions and perspectives are drawn in Sect. 5.

2 Data and methods

2.1 Models description

The two-source energy balance budget, which is similar for both models is firstly described. Then, differences in the solving method and associated assumptions, together with differences in flux parameterization, are briefly reminded.

2.1.1 The two-source energy budget

In the two-source energy balance, total sensible (H) and total latent heat (LE) fluxes arise from the soil and vegetation heat and vapor sources. Applying energy conservation and continuity principles, the energy budget can be described with the following set of equations:

$$H = H_{[soil]} + H_{[veg]} \tag{1}$$

$$LE = LE_{[soil]} + LE_{[veg]} \tag{2}$$

$$R_n = R_{n[soil]} + R_{n[veg]} \tag{3}$$

$$R_{n[soil]} = H_{[soil]} + LE_{[soil]} + G \tag{4}$$

$$R_n = H + LE + G, \tag{5}$$

where G is the ground heat flux and R_n is the net radiation. All fluxes are expressed in Wm^{-2}. The H and LE fluxes expressions are given in Shuttleworth and Wallace (1985, Eq. 6 and 7, p. 843) for a resistive scheme (following analogy with Ohm's law) of a one-dimensional description of energy partition for sparse crops assuming horizontal uniformity. H and LE expressions for the complete canopy between the level of mean canopy fow and reference height can then be written as:

$$H = -\frac{\rho c_p}{r_a^a}(T_x - T_0) \tag{6}$$

$$LE = -\frac{\rho c_p}{r_a^a \gamma}(e_x - e_0) \tag{7}$$

Where γ is the psychrometric constant ($mb\ K^{-1}$), r_a^a the aerodynamic resistance between canopy source height and reference level ($s\ m^{-1}$), e_x and e_0 vapor pressure (mb) at canopy source height and reference height and T_x and T_0 temperature (C) at canopy source height and at reference height. The components elements from soil and vegetation ($LE_{[soil]}$, $LE_{[veg]}$, $H_{[soil]}$, and $H_{[veg]}$) are expressed in the same way according to the associated resistances. Afterwards, the vapor pressure deficit at the canopy source height is introduced. The system now becomes a set of five equations with six unknowns, namely: vegetation temperature $T_{[veg]}$, soil temperature $T_{[soil]}$, canopy-space temperature $T_{[canopy]}$ and the corresponding water vapour pressure $e_{[veg]}$, $e_{[soil]}$ and $e_{[canopy]}$. The next steps of the classical solving of a two-source energy balance system are to express $T_{[canopy]}$ as a function of $T_{[veg]}$ and $T_{[soil]}$ thanks to the continuity equation in H and $T_{[veg]}$ as a function of $T_{[soil]}$ using the energy budget of vegetation. In addition, the heat conduction flux in soil G is either estimated from net radiation (TSEB model) or residual of the energy budget (SEtHyS model) as detailed in the appendix. The solving method consists in the linearization of the equations of the previous system. The basic differences between approaches is that for SVATs models, soil temperatures at different depths are prognostic variables tightly linked to water mass balance, whilst radiative temperature is a forcing input for the SEB models used to infer $T_{[veg]}$ and $T_{[soil]}$ as detailed below.

2.1.2 TSEB

The TSEB model has been first described in Norman et al. (1995) and has been the subject of several refinements. The version of TSEB used in this study is described below. The solving principle is briefly described below. TSEB is forced by a radiometric surface temperature T_{rad} so that soil and vegetation temperatures contribute to T_{rad} in proportion to the fraction of the radiometer field of view (f_θ) that is occupied by each component, thus adding a sixth equation to the system above:

$$T_{rad}(\theta) = [f_\theta \times T_{[veg]}^n + (1 - f_\theta) \times T_{[soil]}^n]^{1/n}, \tag{8}$$

where the factor n is usually fixed to 4 (Becker and Li, 1990). The available energy at the soil surface is computed considering an exponential extinction of net radiation (i.e. Beer's Law):

$$R_{n[soil]} = R_n \times \exp\frac{-\kappa \times LAI}{\sqrt{2\cos\theta}}, \tag{9}$$

where the factor κ is set to 0.45 for spherical distribution of leaves following Roos (1991). The conduction flux in the soil is expressed as a fraction of the available energy at the soil surface :

$$G = \Gamma \times R_{n[soil]}, \tag{10}$$

with Γ an empirical coefficient usually equal to 0.35 (Choudhury et al., 1987). Finally, the resolution of this set of equations relies on the (strong) assumption that, most of the time, vegetation transpires at a potential rate. The Priestley Taylor equation gives a first estimation of canopy transpiration (Norman et al., 1995, Eq. 12):

$$LE_{[veg]} = \alpha_{PT} \times f_g \times \frac{\Delta}{\Delta + \gamma} \times R_{n[veg]}, \tag{11}$$

where α_{PT} is the Priestley Taylor parameter, f_g the green vegetation fraction cover, Δ the slope of the saturation vapor pressure versus temperature curve and γ the psychrometric constant. α_{PT} values ranges between 0.5 and 2.0 (Hssaine et al., 2018) according to meteorological conditions including advections, green fraction of vegetation and soil water availability with an average value around 1.3.

In the "series" resistance network used in this study (see justification below) described in Norman et al. (1995, Fig. 11), the sensitive heat fluxes are expressed as:

$$H_{[soil]} = \rho c_p \frac{T_{[soil]} - T_{[canopy]}}{r_s} \tag{12}$$

between the soil surface and the canopy air space,

$$H_{[veg]} = \rho c_p \frac{T_{[veg]} - T_{[canopy]}}{r_x} \tag{13}$$

between vegetation and canopy air space,

$$H = \rho c_p \frac{T_{[canopy]} - T_a}{r_a} \tag{14}$$

between canopy air space and reference height for atmospherical measurements. Where r_s, r_x and r_a are the associated resistances given respectively in (Norman et al., 1995, Eq. B.1, Eq. A.8, Eq. 6). $H_{[veg]}$ is then computed as the residual of the vegetation energy balance (eq. 1). $T_{[veg]}$ is derived from $H_{[veg]}$; $T_{[soil]}$ from Eq. (8); $H_{[soil]}$ is computed from $T_{[soil]}$ and $LE_{[soil]}$ as a residual of the soil energy balance (Eq. 1). Should $LE_{[soil]}$ be found negative, meaning that there is condensation on the soil surface, which is very unlikely during the day, then the initial value of the Priestley-Taylor coefficient α_{PT} is iteratively reduced until $LE_{[soil]} = 0$ following Anderson et al. (2005) and Li and Kustas (2005).

In agreement with (Li and Kustas, 2005), the "series" layout of resistance (Norman et al., 1995) was found to provide overall more accurate results (not shown) and also less sensitivity to vegetation cover estimate. Furthermore, for model comparison, it was also relevant that both resistance network were similar in TSEB and SEtHyS model.

2.1.3 SEtHyS

The SEtHyS –French acronym for *Suivi de l'Etat Hydrique des Sols* or monitoring of the hydric condition of the soils– SVAT model physics and the main parameterizations are described in Coudert et al. (2006). The main equations of SEtHyS are

Table 1. TSEB parameters (9) with reference values and optimal values obtained from sensitivity analyses.

Category	Parameter	Description [unit]	Litterature range	Reference value	Optimal value
Optical properties	A_{soil}	Soil albedo	0.05 – 0.35	0.15	0.14
	$A_{vegetation}$	Vegetation albedo	0.10 – 0.30	0.3	0.3
	E_{soil}	Soil emissivity	0.94 – 0.97	-	0.94
	$E_{vegetation}$	Vegetation emissivity	0.90 – 0.99	-	0.97
	ϵ	Surface emissivity, involved in CNR1 Ts conversion	0.96 – 0.99	-	0.96
Vegetation characteristics	S	Leaf size $[m]$, involved in computing surface resistance	-	0.01	0.01
	α_{PT}	Priestley-Taylor coefficient, involved in estimating canopy transpiration (Eq. 11)	1 – 2	1.26	1.3 – 1.5
Surface properties	Γ	Soil energy partition coefficient : $G = \Gamma \times R_{n[soil]}$ (Eq. 10)	-	0.35	0.35
	κ	Coefficient of the exponential extinction of net radiation to compute available energy at the soil surface (Eq. 9)	0.3 – 0.6	0.45	0.4

summarized in appendix A. The model belongs to the "two sources, two layers" SVAT model category. Actually, the coupled water and energy budget is solved for the vegetation and soil sources and the soil description for water and heat transfers is based on the force-restore Deardorff formalism (Deardorff, 1978). The model requires atmospheric and radiative forcing and surface biophysical parameters as inputs. It calculates the energy and water fluxes between surface and atmosphere and simulates the evolution of soil and canopy temperatures, air temperature and specific humidity within the canopy, as well as the surface and the root zone soil water content. The heat and water transfer calculation within the continuum soil-vegetation-atmosphere is based on a resistance concept. The resistance network is made of four nodes: the reference height for the low atmospheric weather forcing; inside the vegetation at the displacement height plus the roughness length; just above ground at the soil roughness length; and, at ground level. The aerodynamic resistances –above and inside vegetation canopy– are determined with the wind speed profile description inside the canopy from Shuttleworth and Wallace (1985) and Lafleur and Rouse (1990). The evapotranspiration calculation takes into account partition between free water in the canopy and the rest of the leaves (Monteith, 1965; Deardorff, 1978) and is based on the stomatal resistance for "big leaf" model from Collatz et al. (1991). The vegetation photosynthesis and stomatal resistance parameterizations are the same as those used by the SiB model (Sellers et al., 1996). The soil hydrodynamic properties to calculate water transfer processes within the soil porous network are given by Genuchten (1980). Ground heat flux conduction is obtained as the residual of the soil energy budget. Finally, the radiative transfer model included in the model for TIR domain (François, 2002) allows simulating brightness temperature and

Table 2. SetHyS parameters (22) with initial uncertainty ranges used for MCIP calibration.

Category	Parameter	Description [unit]	Initial uncertainty range
Optical properties	E_g	Bare soil emissivity	0.94 – 0.99
	A_{sec}	Dry soil albedo	0.225 – 0.35
	A_{hum}	Wet soil albedo	0.1 – 0.22
	W_{inf}	Moisture parameter for albedo calculation	0.15 – 0.29
	W_{sup}	Moisture parameter for albedo calculation	0.291 – 0.5
	A_{sv}	Vegetation albedo	0.16 – 0.32
Vegetation characteristics	V_{max0}	Leaf photosynthetic capacity (Rubisco) [$\mu mol\ m^{-2}\ s^{-1}$]	30 – 200
	l_{gf}	Dimension of the leaf along the wind direction [m]	0.01 – 0.08
	k_{wstr}	Empirical parameter for water stress calculation	0.01 – 0.1
Ground properties	p_{hc}	"Half critic" hydrologic potential [m]	-200 – 100
	W_{max}	Saturated soil water content [$m^3\ m^{-3}$]	0.3 – 0.5
	W_{resid}	Residual soil water content [$m^3\ m^{-3}$]	0.05 – 0.15
	h_{VG}	Scale factor in the Van Genuchten retention curve model [m]	-1.161 – 0.251
	n_{VG}	Shape parameter in the Van Genuchten retention curve model	1.168 – 1.331
	K_{sat}	Saturated hydraulic conductivity [$m\ s^{-1}$]	2.4×10^{-8} – 2.7×10^{-6}
	a_{Elim}	Empirical parameter for limit evaporation	1 – 50
	b_{Elim}	Empirical parameter for limit evaporation	1 – 50
	F_{therm}	Correction coefficient of the volumetric soil heat capacity [$J\ m^{-3}\ K^{-1}$]	0.5 – 2
	dp_2	Root zone depth [mm]	200 – 2000
Initialization variables	w_{g0}	Initial soil surface water content [$m^3\ m^{-3}$]	-
	w_2	Initial root zone water content [$m^3\ m^{-3}$]	-
	$bias_{T2}$	Error in deep soil temperature [K]	-2 – 2

radiative temperature, and thus gives the possibility of constraining the model with TIR data (Coudert and Ottlé, 2007; Coudert et al., 2008). The SEtHyS model requires a set of about 22 parameters presented in Table 2.

Figure 1. Experimental sites localization in France (left) and Morocco (right).

2.2 Sites description and data

The experimental data set has been gathered in South West of France (Béziat et al., 2009) and South East of Morocco (Chehbouni et al., 2008; Jarlan et al., 2015) as shown in Fig. 1. As presented in Table 3, all necessary data to run, calibrate and evaluate models were collected over 3 agricultural sites, spanning a total of 7 cultures cycles from seeding to harvest: 3 wheat (*Triticum aestivum L.*) crops, 1 sunflower (*Helianthus annuus L.*) crop and 2 corn (*Zea mays L.*) crops. Experimentals sites differ by different management practices (culture rotation and irrigation), soil properties, topography and climates (6 temperate crop cycles and 1 semi-arid crop cycle). Auradé (43.55°N, 1.11°E) and Lamasquère (43.50°N, 1.24°E) experimental sites are located near Toulouse in south-western France and are part of the "SudOuest" project (Dedieu et al., 2001; Béziat et al., 2009). Both experimental sites are under influence of temperate climate. A rotation of wheat and sunflower is cultivated in Auradé, while a rotation of wheat and irrigated corn is cultivated in Lamasquère. Complete description of site features and data sets are presented in Béziat et al. (2009). Sidi Rahal (31.67°N, 7.60°W) experimental site is located in the Haouz plain in central Morocco and is part of the "Sud-Med" project (Chehbouni et al., 2008; Jarlan et al., 2015). It is part of an irrigated agricultural area under influence of a semi-arid climate, where wheat is the most widely grown crop. More information about site and data set is given in Duchemin et al. (2006).

Each experimental station collected standard meteorological data at a half-hourly time step intervals: Global incoming shortwave and longwave radiation (R_g and R_a), wind speed (U_a), air temperature (T_a), atmospheric pressure (P_a), relative humidity (R_h) and rainfall. The four components of the net radiation (R_n) were measured using a CNR1 radiometer (Kipp and Zonen, Delft, NL). Land surface temperature (LST) was computed from measured upward and downward long wave components of the net radiation, using Stefan-Boltzmann's law and an estimation of surface emissivity (Becker and Li, 1995). Sensible (H) and latent (LE) heat fluxes were measured continuously using Eddy-Covariance (EC) systems (Moncrieff et al., 1997; Aubinet et al., 2000). Fluxes were processed with classical EC filters and corrections (Béziat et al., 2009). Accuracy on

flux estimates is expected to range between 5 $\%$ and 30 $\%$ (Eugster et al., 1997; Wilson et al., 2002). Soil heat flux (G) was sampled using heat flux plates located at depths ranging from 5 cm to 1 m. Automatic measurements were then complemented by vegetation sample. Vegetation height (h_c) and green Leaf Area Index (LAI) were collected periodically along crop cycles and interpolated using Piecewise cubic Hermite algorithm. Green LAI was determined from destructive measurements with a LiCor planimeter (LI3100, LiCor, Lincoln, NE, USA). In order to obtain estimation of fraction of green (f_g), total LAI (LAI_{green} + LAI_{yellow}) was extrapolated from green LAI data, applying a linear decrease starting at the LAI maximum and ending at harvest with a value of $LAI_{total} = 0.8 \times LAI_{max}$. In order to assess the potential loss of accuracy of meteorological inputs at the landscape scale and impact on model simulations, SAFRAN reanalysis data (Quintana-Seguí et al., 2008) are used within this study. SAFRAN is based on an optimal interpolation between a background estimate obtained from Météo France's Numerical Weather Prediction Model (ALADIN) and weather station observations, except for precipitation relying on the ground station network only and for the incoming radiation fluxes (downwelling surface shortwave and longwave) which are computed from Ritter and Geleyn's radiation scheme (1992) from the outputs of a numerical weather forecast model and the solar constant at the top of the atmosphere (for shortwave incoming radiation). Data was kindly provided by Météo-France.

2.3 Assessing the model skills

Keeping in mind that we plan to spatialize a SVAT model, whose parameters are highly dependent on growth stage of vegetation, we must be able to determine sets of parameters representing specific phenological stages and hydric conditions (stressed/non-stressed). For this reason evaluation is not performed continuously over the whole crop cycles, but specific periods of interests were identified to assess the model skills. These periods were chosen to be ten days long in order to catch synoptic scale variability of the weather, as shown by Eugster et al. (1997) with the help of spectral analysis. This duration is also short enough to remain representative of a specific phenological stage, and long enough to gather a sufficient amount of data. For each crop cycle, four specific study periods were chosen, each corresponding to the following phenological stages: rising/emergence stage ($0.1 < LAI < 0.3$), growth stage (rapid increase of LAI and $LAI \approx 1$), maximum development stage (around LAI maximum value) and senescence stage (LAI decreases). Starting days of periods were adjusted to optimize the quality of available data, as the data sets are subject to sporadic measurements issues and energy closure inconsistencies (filtered to a minimum of 80 $\%$).

In order to better assess the differences of model skills during stress periods, water stress is quantified along the whole crop cycles using two indicators:

- the Evaporation Stress (SE, Boulet et al., 2007) related to the ratio between real and potential evapotranspirations:

$$SE = 1 - \frac{LE}{LE_{pot}}, \tag{15}$$

  where LE_{pot} was computed using the Penman-Monteith equation (Canopy resistance was estimated following Jarvis (1976) formulation with a minimum value of 90 $s.m^{-1}$).

– the Soil Wetness Index (SWI, Douville, 1998, among others) of the root zone ranging from 0 at wilting point to 1 at field capacity:

$$SWI = \frac{W_2 - W_{wilt}}{W_{fc} - W_{wilt}}, \tag{16}$$

with W_2 the root zone water content, W_{fc} the water content at field capacity, and W_{wilt} the water content at wilting point.

As cultures from our data set are irrigated or in temperate areas, most stress periods are found during senescence phases, when water resources are low or irrigation is stopped. The model skills are assessed through classical statistical metrics including Root Mean Square Error (RMSE), Mean Absolute Percentage Deviation (MAPD), bias and determination coefficient r^2.

2.4 Implementation of the models

Considering our objective to compare a complex SVAT model with the TSEB tool taken as an example of a simple and robust approach, a different strategy has been applied for the implementation of the two models. The 22 parameters of the SEtHyS model were finely tuned for each crops and each phenological stages. The objective of this calibration was not to fit the data at best but rather to evaluate the sensitivity of model outputs to potentially poorly calibrated parameters when the model is to be applied to an heterogeneous agricultural landscape at the field or intra-field scale. To this objective, four different cases corresponding to four different sets of parameters are considered to quantify the potential loss of performances due to wrong parameter values. The four cases are listed below from the "best" conditions when the parameters are calibrated for each site, each crop and each phenological stage to the worst when generic values are used:

1. Site and period specific parameters sets (hereafter named "optimal") for each site, crop class (i.e. type of culture) and phenological stages. Note that the analysis of the model skills (Sect. 3.1) is performed using this parameters set.
2. More generic parameters sets depending on crop class and phenological stages only (named hereafter "pheno+cult").
3. If no information is available for characterizing phenology, a calibrated set of parameters for the whole cultural crop cycle is computed (hereafter named "culture only").
4. The last case corresponds to the "optimal" parameters set but applied to another crop class in order to take into account potential errors that are likely to occur when working with a land-use map (named "unadapted").

What we consider the "best" case is very unlikely for a spatialized application of the tool because the largest the available database, it will never cover all the conditions encountered at the scale of an heterogeneous agricultural landscape where each plot has its specific soil, technical itinerary, hydric status, etc... Our objective is thus to get different parameters sets with values close to what is expected for each type of conditions (crops, climate, sites, phenological stages...) but without giving too much importance to the values themselves. To help perform the calibration, a stochastical multi-objective calibration method (Multi-Objective Calibration Iterative Procedure or MCIP; Demarty et al., 2004, 2005) has been implemented in order to minimize

RMSE between simulations and measurements at half-hourly time intervals. Five objective functions are identified: RMSE of H and LE fluxes, surface brightness temperature (T_b), net global radiation (R_n), and root zone soil water content (SWC). An ensemble of simulations based on a monte-carlo sampling of the parameter space is carried out, and the objective functions are optimized jointly following a Pareto ranking. The basic principle is that a simulation is classified "better" than the others if all the objective functions have lower values. For more details, the MCIP methodology is described in Demarty et al. (2004, 2005).

For TSEB, the most robust configuration of the model is sought. To this objective, as a first step, the most sensitive parameters (Diarra et al., 2017) for convection fluxes prediction are calibrated on the whole database at once. These parameters are the Priestley Taylor coefficient (α_{PT}), the coefficient of net radiation extinction (κ), and the empirical coefficient (Γ) relating $R_{n[soil]}$ to G. The objective functions are the RMSE of H and LE. Those calibrated values are reported at table 1. They are almost the same as those proposed by Norman et al. (1995) and will be kept for the TSEB runs in the next section of the paper. A more optimal calibration by crops, site and phenological stages has also been carried out (not shown). Main finding can be summarized as follows:

1. The RMSE difference between Norman et al. (1995) values and the optimal one calibrated for each crop and stage didn't exceed 10 Wm^{-2} on LE. In addition, most of optimal κ values range between 0.38 and 0.58; the only notable exceptions are fully covering wheat with lower interception (κ value around 0.3) that may be attributed to the erectophile distribution of wheat leaves and fully covering maize and sunflower characterized by a higher interception (κ values reaching 0.7).

2. Likewise, the RMSE difference between initial Norman et al. (1995) and the optimal ones for the α_{PT} parameter remain below 6 Wm^{-2} except during the senescence stages where they can reach more than 35 Wm^{-2}. Errors by taking the literature value of 1.3 are thus very limited. Finally, the range of optimal values is relatively narrow (1.05 to 1.6).

3. For the Γ parameter, differences of RMSE between the optimal values and 0.35 proposed by Norman et al. (1995) are below 8 Wm^{-2} apart from the rising stage where we observed errors up to 79 Wm^{-2} on the sunflower site. Values range between 0.05 and 0.7.

Still with the goal of identifying the most robust configuration of the TSEB model, several refinements proposed by different authors to improve models prediction for specific crop and climate conditions were also tested with our database. The Priestley-Taylor formulation yet relatively simple provides accurate potential transpiration in a wide range of conditions but neglect the aerodynamic resistance. Colaizzi et al. (2014) proposed to replace the Priestley-Taylor expression by the Penman-Monteith equation (Monteith, 1965) in particular for advective conditions thus avoiding to increase the value of the α_{PT} parameters as proposed by Kustas and Norman (2000) for such conditions. Unfortunately, the Penman-Monteith version worsened the results of about 6.3% on average on the whole data base and was not retained in this study. Several parameterizations aiming to represent the diurnal course of Γ have also been proposed. Those of Santanello et al. (2003) and of Chávez et al. (2005) have been tested. The overall performance of the model to predict convective fluxes were slightly worsened on average apart for some very specific conditions. Interestingly enough, a multiplicative factor to κ lower than 1 has been proposed by Campbell

and Norman (1998) in the divergence equation (eq. 9) to take into account the clumping of some crops that may intercept a lower part of the incoming radiation than if leaves were randomly distributed (Kustas and Norman, 1999). The calibrated values of κ for sunflower and maize are above 0.45 proposed by Norman et al. (1995) (cf. point (1) above). This tends to show that a higher fraction is intercepted probably because of a dominantly planophile distribution of leaves for both crops rather than a clumping effect. Finally, the simple radiative transfer model of Kustas and Norman (1999) has been tested as an alternative to Beer law proposed by Norman et al. (1995). Although close on average (RMSE differences on $Rn < 17\ Wm^{-2}$), significantly worse RMSE were obtained during the rising stage on wheat and sunflower.

3 Results

3.1 Models skills by crops and phenological stages

Model simulations of heat fluxes are compared to tower fluxes measurements at half-hourly and daily time steps, with a focus on performance by crops and by growth stage. RMSE's for LE, H and R_n are displayed in Table 4 and MAPD's for H and LE are displayed in Fig. 2. Biases (not shown) are very limited and ranged between -23 Wm^{-2} and +10 Wm^{-2} for both models, except during the rising phase where they reach -47 Wm^{-2} and +43 Wm^{-2} for SEtHyS and TSEB, respectively (see discussion below). Available energy is well simulated for both models with daily averaged RMSEs of 43 Wm^{-2} and 19 Wm^{-2} for TSEB and SEtHyS, respectively.

Regarding heat fluxes, Table 4 points out good performances of the TSEB model on daily averaged values despite the relative simplicity of the approach compared to SEtHyS, which relies on a systematic parameter calibration. Both models exhibit close statistics concerning LE estimations (RMSEs of 35.5 vs 38.9 Wm^{-2} for SEtHyS and TSEB, respectively) while TSEB behaves slightly better regarding H estimations (21.2 vs 28.7 Wm^{-2}). These values are close to errors found in the literature for TSEB (Norman et al., 1995; Zhan et al., 1996; Anderson et al., 1997; Kustas and Norman, 1999; French et al., 2005; Kalma et al., 2008; Diarra et al., 2013, 2017) and also within the range of expected errors from EC towers measurements (Eugster et al., 1997; Wilson et al., 2002). Half-hourly values lead to similar conclusions, except that the drop in retrieved LE's performance associated to this change of reference time interval is stronger for TSEB than for SEtHyS. Interestingly enough, this first analysis hilights important disparities in terms of LE prediction skills between the various growth stages. Indeed, Fig. 2 highlights some regularity in the SEtHyS skills regardless of growth stages and crops, as evidenced by the narrow group formed by the SEtHyS points. By contrast, the range of MAPD values for TSEB is much wider. In particular, limitations of the model are clearly emphasized during rising and senescence stages. During the senescence phase, these discrepancies may both be attributed to stress (see discussion below) but could be related also to a poor partition of available energy between soil and vegetation. Indeed, the change in the radiative features of the canopy, including albedo, which occurs on senescent plants, is not taken into account by the model. However, regarding irrigation practices, it should be noted that assessing accurate ET during senescence is not as important as during the growth season.

The poor performance during the rising stage is due to excessive limitation of the soil sensible heat flux, induced by the parameterization of the roughness length for momentum ($Z0m = h_c/8$) at the denominator of the expression of the aerody-

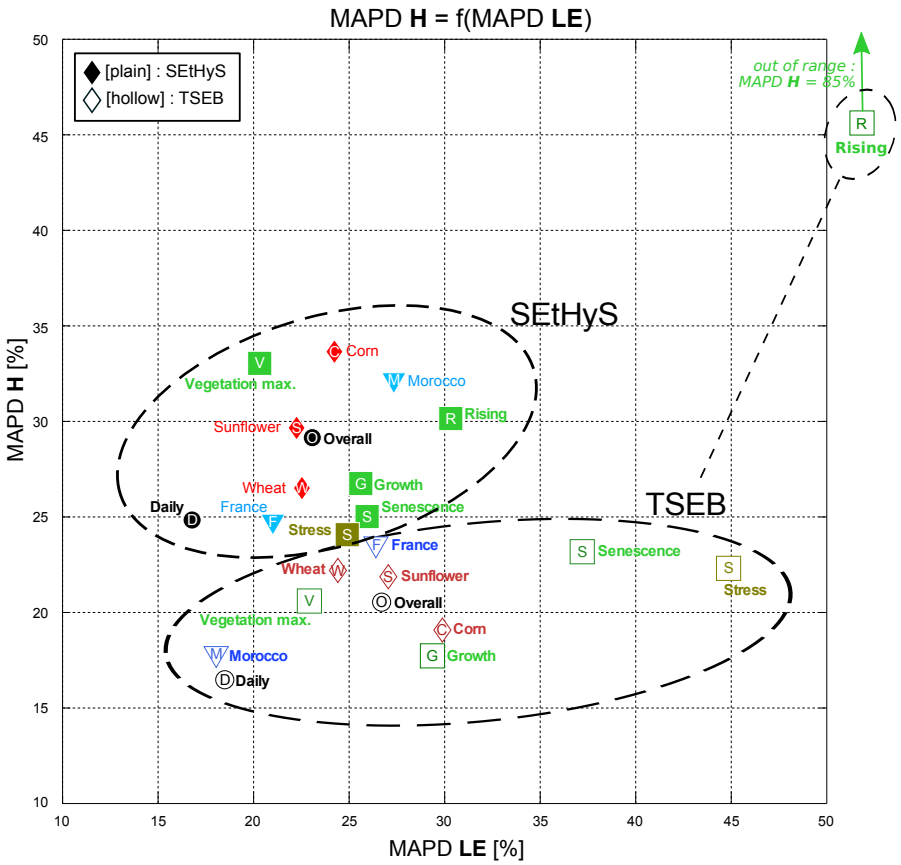

Figure 2. Comparison of TSEB (hollow markers) and SEtHyS (plain markers) estimations of H and LE for various time resolutions (circles), phenological stages (squares), cultures (diamonds) and climates (triangles). SEtHyS results are computed with the "optimal" sets of parameters (see Sect. 2.4). MAPD stands for Mean Absolute Percentage Deviation.

namic resistance r_a, leading to very high resistance when canopy height is very low. Since, during that stage, the vegetation net radiation is very limited, vegetation sensible heat is also close to 0. The observed high MAPD of LE during the rising phase shall thus be attributed to significant bias of TSEB estimates. To a lesser extent, SEtHyS skills are also mitigated during the rising phase. Generally, when evaporation is predominant over transpiration, more weight is given to soil transfer processes which are harder to characterize, considering the high heterogeneity of soil characteristics and the limited soil measurements available for calibration. The poor performances are more conspicuous with TSEB leading to estimation of H with a MAPD of 85 %. By contrast, both models tend to have better performance when vegetation is fully-developed (MAPD less than 23 % for LE). The model performance by crop and growth stage is detailed in Fig. 3 (a) and (b), respectively, as normalized Taylor diagrams (Taylor, 2001). This diagram is a concise way to display the ratio between the variances of the model outputs and the observed data, the correlation coefficient r and the RMSE between model estimates and observations normalized by the variance of the observed data set. The further from the point marked “observed reference” on the abscissa axis, the higher

the normalized RMSE; likewise, dots on the right (left) side of the circle cutting the ordinate axis at "observed reference" overestimates (underestimates) the observation variance. Figures 3 (a) and (b) point out higher normalized standard deviations for TSEB LE estimations. These noisier outputs are likely due to the instantaneous ("snapshot") computing architecture of the model, while SEtHyS is better constrained by its continuous evolution of the soil water content which lead to smoother predictions of the daily cycle. This explains the drastic drops of TSEB RMSE on LE when going from daily to half-hourly observations already underlined above. Finally, no significant skill differences are observed between crops, which seems to indicate that (1) the set of parameters used in TSEB describes well vegetation characteristics and that (2) the SEtHyS formalism can be adapted to various crops, provided that parameters are properly calibrated. More focus on the selected sets of parameters is given in the discussion section. Models performs well in both climate: SEtHyS showed slightly better performances for flux estimates in France (MAPD for LE of 23 $\%$ in France and 30 $\%$ in Morocco), whereas TSEB showed slightly better performances for flux estimates in Morocco (MAPD for LE of 26 $\%$ in France and 18 $\%$ in Morocco). However, differences in crop management between France and Morocco and the availability of only one crop cycle in Morocco does not allows to draw final conclusions about climate impact on model skills. TSEB has lower performances on senescence periods (including hydric stress) for LE estimation (MAPD of 45 $\%$). This is partly due to Priestley-Taylor approximation which is suitable for unstressed vegetation in potential conditions (Priestley and Taylor, 1972), and to the fact that it does not have a water budget description. Increased LST resulting from water stress does not allow limiting LE significantly enough in the TSEB scheme (see Sect. 3.2.7). Several authors have already pointed out that TSEB do not faithfully reproduce periods of senescence and water stress (Kustas et al., 2003; Crow et al., 2008; Boulet et al., 2015). SEtHyS includes description of soil water transfers and leaf processes –in particular stomatal resistance– and can better reproduce hydric stress impact on LE flux (MAPD of 28 $\%$).

3.2 Sensitivity analyses to inputs

3.2.1 Overview

Given the overall purpose of our research dedicated to the spatialized estimation of evapotranspiration at various scales, quantifying the decrease of model performance due to deterioration of input data quality combined with change of spatial scale from the field to a heterogeneous agricultural landscape is a prerequisite. Applying the models at the landscape scale is not performed the same way for both approaches: TSEB is designed to be driven by remote sensing data with ET computed directly at the resolution of the TIR pixel, while SEtHyS is spatially distributed by computing fluxes at the crop scale for each homogeneous entities separately. As a consequence, both models' performances are expected to exhibit sensitivity to the quality of auxiliary spatialised meteorological and vegetation forcing variables, TSEB's performances are expected to depend on the quality of the TIR data, and SEtHyS's performances are expected to depend on the quality of the description of the state of each homogeneous entity (i.e. soil water content initialization, and sets of parameters describing soil properties and vegetation behavior).

The specific purpose of this section is twofold: (1) identify the most sensitive inputs and (2) quantify the expected model perfor-

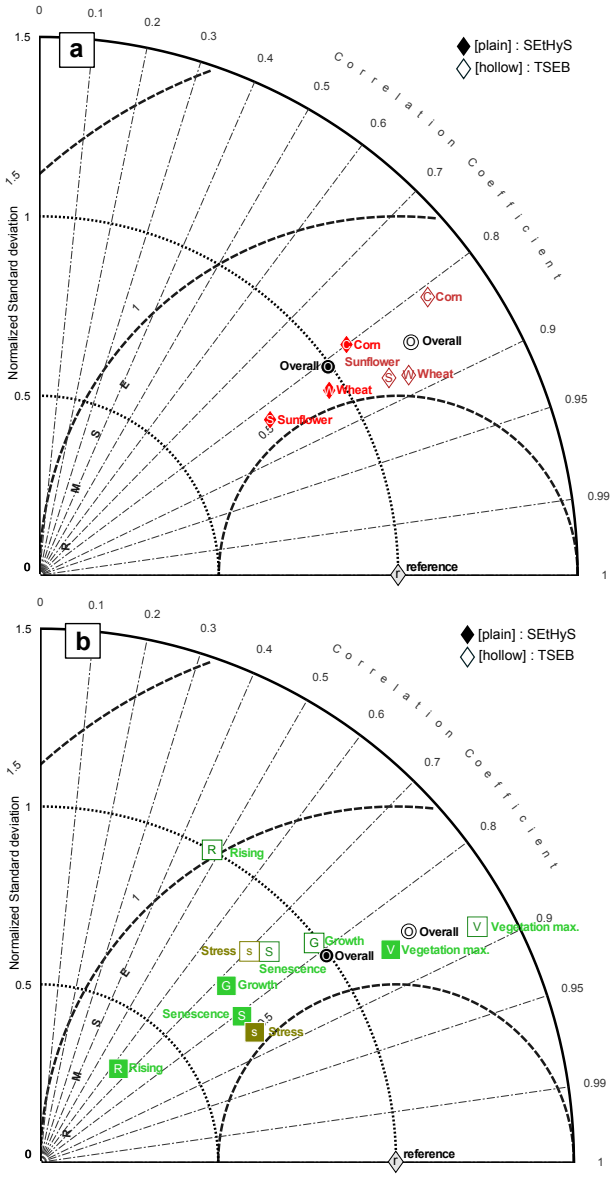

Figure 3. Taylor diagram for LE performances of TSEB (hollow markers) and SEtHyS (plain markers). Top diagram (a) compares various cultures, bottom diagram (b) focuses on phenological stages. Concentric lines centered on 0 indicate the normalized standard deviation with observations, radial lines indicate the correlation coefficient between simulations and observations, normalized RMSE isolines are the concentric circles centered on "r" (reference for the overall time series of observations: RSME=0, corr. coeff.=1 and NSD=1).

mances when realistic input errors are introduced. Expected uncertainties on input variables have been evaluated by comparing available *in situ* data to the spatialized data sets (SAFRAN meteorological reanalysis and ASTER, LANDSAT, FORMOSAT2 satellite imagery and products). Results are presented in Table 5 and details are given in the following sections.

3.2.2 Intercomparison of SAFRAN and *in situ* meteorological data

Comparison results between the two available meteorological stations in the South-West France and the closest SAFRAN 8-kms grid points (inverse interpolated distance) are reported in Table 5 in terms of RMSE and biases (2006–2008 period). On average, SAFRAN provides consistent results for air temperature and relative humidity, with reasonable RMSE and biases close to 0. To a lesser extent, wind speed is also well reproduced although slightly biased. The SAFRAN ability to predict incoming radiation is less convincing: bias is low but RMSE reaches 90 Wm^{-2} (about 20 $\%$ on average). This comparison corroborates the conclusions of Quintana-Seguí et al. (2008) who also highlight a strong weakness of SAFRAN in terms of incoming radiation predictions. Er-Raki et al. (2010) used a forecast model (ALADIN from Météo-France) over the Tensift basin of Morocco. The results showed that the ALADIN forecasts are in good agreement with the station measurements in terms of solar radiation (R_g) and air temperature (T_a). However, the comparison of the station and the forecasted values of relative humidity (R_h) and wind speed (U_a) are much more scattered. Besides the RMSE and biases representing time averaged statistical characteristics of the difference between SAFRAN and the two ground stations, it is also interesting to consider more extreme error values. To do so, the 1^{st} and 9^{th} deciles of the difference distribution are shown in Table 5 in absolute values and in percentage. The probability of occurrence of such errors is far from insignificant as 20 $\%$ of the data are involved. These "extreme" errors are considered for the sensitivity study regarding (1) the instantaneous estimates provided by the TSEB model depending on satellite overpass time, leading to potential instantaneous errors much higher than the average; (2) the poorest quality of re-analysis data in the semi-arid areas because the meteorological station network may be scarcer.

3.2.3 Sensitivity analysis to meteorological inputs

Impact of realistic and more extreme errors on convection fluxes simulations are shown in Fig. 4 and Fig. 5, respectively. Focusing on noise (Fig. 4) is of interest since biases are often limited on re-analysis systems thanks to bias reduction procedures. On average, SEtHyS simulations are less sensitive to noisy inputs for LE than for H, whereas reverse conclusions can be drawn for TSEB. Adding white noise to meteorological inputs with the objective of scaling up to agricultural landscape with realistic error has almost no impact on RMSE for SEtHyS when compared to the reference simulation for latent heat predictions. Nevertheless, wind speed has the greater impact on LE with an increase of 10 $\%$ on LE RMSE. As a difference, a realistic level of white noise added to incoming radiation and, to a lesser extent, air temperature, deteriorates TSEB predictions with RMSE of LE simulations lowering from reference value of 55 Wm^{-2} to nearly 60 Wm^{-2}. Indeed, whereas the partition between latent and sensible fluxes is moderated by the slow-varying soil moisture content in SEtHyS, TSEB partition relies on measured available energy and surface temperature inputs only. By contrast, noisier wind speed, air temperature and, to a lesser extent, solar radiation, deteriorate significantly sensible heat for SEtHyS. TSEB appears, on average, less sensitive to noisy meteorological inputs for H. When considering extreme errors (Fig. 5) on meteorological forcing, the same variables are identified as the most sensitive ones: R_a, R_g and T_a for TSEB and R_a, R_g and R_h for SEtHyS. However, whilst SEtHyS performance remains acceptable despite these high errors on forcing, TSEB performance for both LE and H collapse in response to incoming radiation errors in particular. Interestingly enough, incoming solar radiation can also be retrieved from

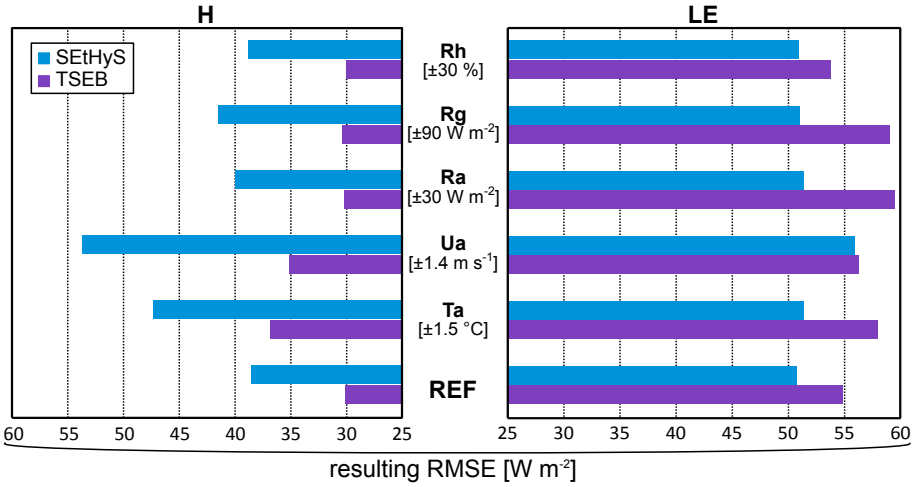

Figure 4. Sensitivity analysis (realistic white noise) to meteorological inputs for both models and impact on estimation of H & LE.

satellite measurements such as MSG. In particular, Carrer et al. (2012) points out a significant improvement of MSG derived short wave and long wave downwelling surface radiation with regards to the SAFRAN analysis system, which could represent a valuable alternative for regional assessment of evapotranspiration. To limit the sensitivity to T_a and absolute surface-air temperature differences, time differencing modeling schemes were developped (Anderson et al., 1997; Norman et al., 2000) with particular interest for large scale applications, provided early morning atmospheric soundings and/or at least two near acquisitions of T_{rad} are available.

3.2.4 Sensitivity analysis to vegetation forcing inputs

Focus here is put on evaluating the bias effect on SEtHyS and TSEB flux predictions. Indeed, on one hand, errors on vegetation characteristics are much more difficult to evaluate as *in situ* measurements are time-consuming and therefore not always available at a small time interval. On the other hand, biases on satellite estimates are more likely to occur than white errors because of a detection limit of visible sensors in the case of sparse vegetation and a possible saturation effect when Leaf Area Index is above 3 $m^2\ m^{-2}$. On average, Claverie et al. (2011, 2012) highlight a potential bias of 20 $\%$ for LAI estimated from FORMOSAT data. Canopy height (h_c) is not available directly from remote sensing data but can be estimated from LAI. Canopy height (h_c) was deduced from $LAI = f(h_c)$ relations, applying linear regression to each culture and phenological stage available in our *in situ* data. This methodology provides estimations of h_c with a MAPD of 30 $\%$, and "extreme" bias up to 100 $\%$ (Bigeard, 2014). The results shown in Fig. 5 demonstrate that TSEB and SEtHyS sensitivity to bias on LAI remains limited. By contrast, TSEB and, to a lesser extent SEtHyS, exhibit a much higher sensitivity to bias on canopy height (h_c) due to erratic transfer resistances when h_c is too close to the height of the micrometeorological measurements, or when soil is considered bare ($h_c = 0$). As LE is computed from the residual of the energy budget in TSEB, a problem is observed on both H and LE fluxes, while LE is less affected in SEtHyS (not shown).

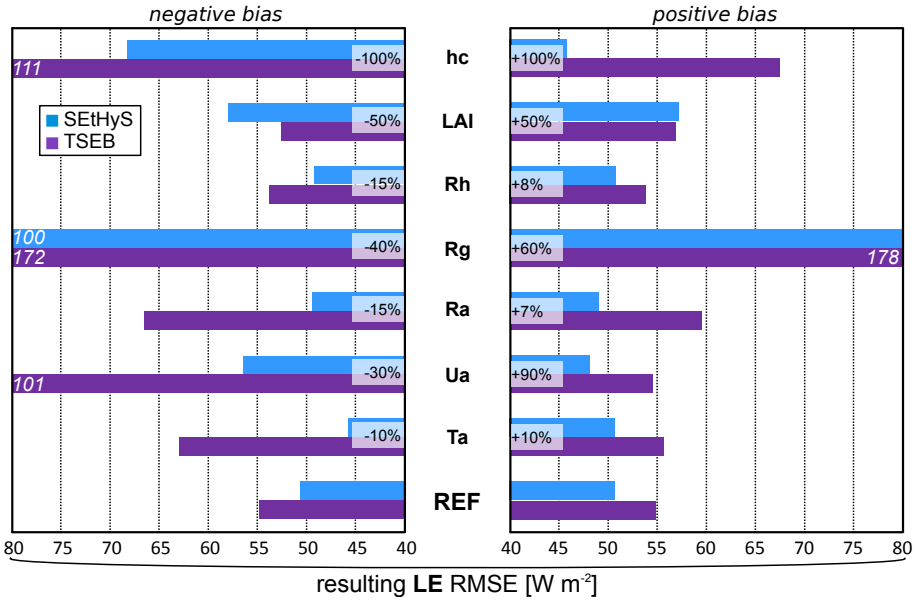

Figure 5. Sensitivity analysis to positive and negative realistic biases applied to meteorological and vegetation inputs for both models.

3.2.5 Sensitivity analysis to radiative temperature for TSEB

The comparison between *in situ* LST measurements and retrieval from the LANDSAT7 and ASTER images yielded a maximum absolute difference of 2.2 K (4 points) in agreement with values reported in the literature ranging from 1 to 3°C (Hall et al., 1992; Gillespie et al., 1998; Schmetz et al., 2002; Peres and DaCamara, 2004; Li, 2004; Liu et al., 2006; Wan, 2008, among others). As LST is expected to be a determining input of TSEB, an in-depth sensitivity analysis to this variable was carried out considering white noise and biases of 1, 2 and 3°C. Indeed, the spatial scale mismatch between the spatial sensor operating, at best, at 90m resolution and the SVAT model operating at the scale of an "agricultural unit" (potentially lower than a parcel) is likely to be important. Regarding the strong heterogeneity of agricultural landscape (in terms of crops, development stage, irrigation, hydric stress, etc.), bias is also likely to be important and quite impossible to correct. The results of adding errors to measured radiative temperature on TSEB fluxes prediction are shown in Fig. 6. For limited white noise up to 2 K, the drop of TSEB skills is small on both H and LE. By contrast, biases are much more impacting. In particular, a negative bias of 3 K could deteriorate LE RMSE from 58 Wm^{-2} to 78 Wm^{-2}. Interestingly enough, a negative bias, that is likely to occur when the observed pixel is partly irrigated (i.e. cold), while the agricultural unit studied lay under stress (i.e. hot) for instance, has a stronger effect than a positive bias. This is likely to occur in many cases in practice: a mixed pixel including forest and stressed field, irrigation heterogeneity within a pixel (for instance in progress irrigation within a field including gravity or center pivot system or the use of a localized sprinkler).

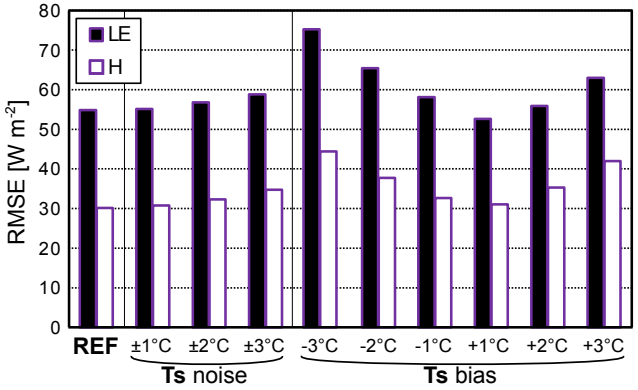

Figure 6. Sensitivity analysis to radiative temperature input for TSEB.

3.2.6 Sensitivity analysis to water inputs and soil water content for SEtHyS

Water inputs, i.e. rainfall and irrigation, are difficult to assess accurately over an agricultural landscape as long as the considered spatial scale exceeds one km^2. Even in this case, a good knowledge of irrigation input at the field level requires costly field surveys, since farmers' associations or regional offices responsible for irrigation water often work at a larger scale made of several plots. In addition to this potential uncertainty, the initial condition of soil water content (SWC) should also be considered uncertain as a result, for instance, from errors piling up from previous inputs. Figure 7 shows results of sensitivity analysis to these three factors: uncertainty on irrigation amount and timing and on SWC initial condition. Unsurprisingly, all factors had a significant impact on LE predictions. Even if input timing was correct, a bias of 1 mm with correct initial SWC deteriorated the SEtHyS skill by 5 $\%$. If the bias on input reaches 10 mm and the initial SWC is negatively biased with the same level, the loss of model performance is above 25 $\%$. Considering that the total amount of an irrigation round can reach 100 mm, a 10 mm uncertainty is very likely to occur in practice. In addition, a negative bias on SWC impacts significantly more LE predictions than a positive bias. Indeed, going towards drier conditions may lead to stress and, as a consequence, to a drastic drop of predicted LE compared to reference, whereas increasing SWC when the surface is already close to potential conditions won't have any effect on LE. Within this context, data assimilation of surface soil moisture retrieved from spatial sensors could provide an interesting solution to improve accuracy of SWC initial conditions (Prevot et al., 1984; Demarty et al., 2005; Li et al., 2006). By contrast, the timing, although important, has a secondary influence on model skills. Even when water input is applied 3 days before or after the actual date, the loss of LE predictions skills remain limited at around 15 $\%$. Indeed, considering that agricultural landscape is often well-watered in order to maximize production, vegetation is able, through transpiration processes, to maintain high levels of LE during long periods. The resulting dynamics of LE is relatively smooth compared to bare soil that is dominated by evaporation processes. Finally, the main conclusion is that emphasis should be laid on a water amount prescription whilst timing appears of secondary importance.

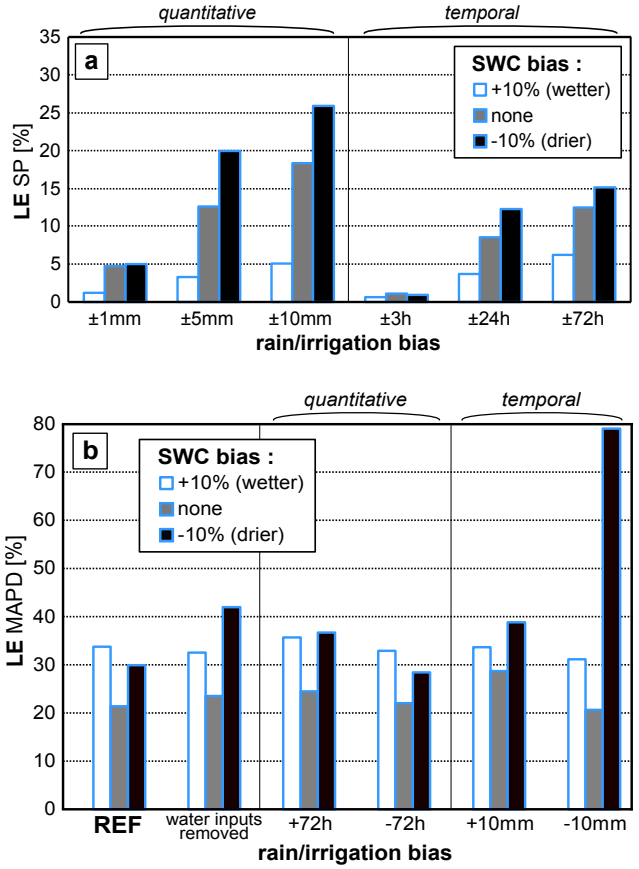

Figure 7. SEtHyS sensitivity analysis to rain and irrigation inputs, with influence of bias on Soil Water Content (SWC). SP in figure (a) is defined as $SP = \frac{|LE_{[positivebias]} - LE_{[negativebias]}|}{LE_{[reference]}}$.

3.2.7 Cross sensitivity analyses of models through linkage of radiative temperature and SWC

Sensitivity of the TSEB and SEtHyS models to surface water status has to be detailed in order to compare how the models respond to a change in water conditions. The difficulty lies in the conceptual difference between both models: surface water status is an explicit variable state for SEtHyS while, in the TSEB model, surface radiative temperature is an indirect proxy of the surface hydric conditions. For the set of simulation periods considered in this study, initial soil water contents (for surface and root zone) were biased in SEtHyS inputs with +/-10, +/-30 or +/-50 % levels. As a consequence, the simulated radiative surface temperature by SEtHyS diverges from reference and the differences between both temperatures simulations time-series are added to the TSEB model input radiative temperature as an equivalent water bias converted in temperature. It is assumed that the SEtHyS model, used with a calibrated set of parameters, is able to simulate a realistic temperature equivalent to the water status biases (Coudert et al., 2006; Coudert and Ottlé, 2007). Figure 8 shows the average variation of the temperature bias as a function of the SWC bias. As expected, temperature increases with water content deficit. Beyond the [-10 % – +10 %] interval,

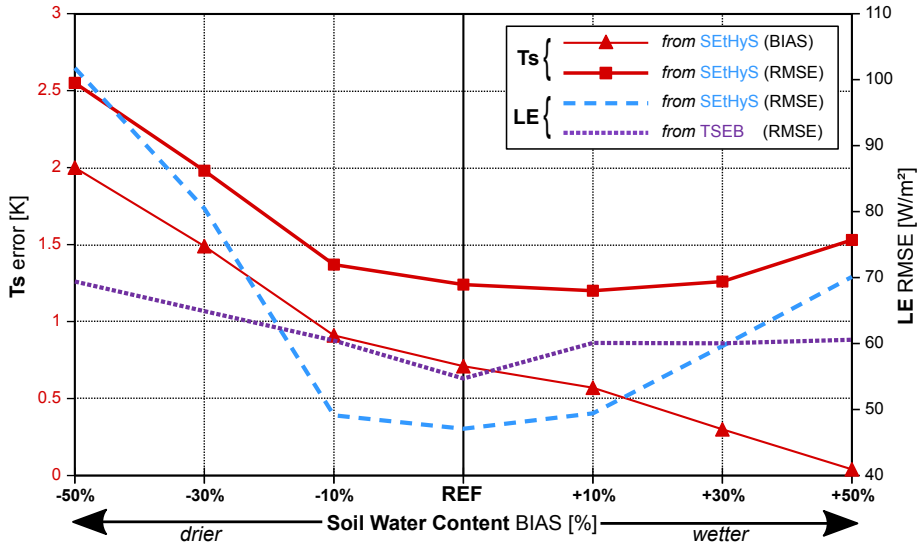

Figure 8. Error of Ts simulated by SEtHyS for increased and decreased SWC, and impact on models LE estimates. TSEB is forced with Ts estimates from SEtHyS.

temperature and water contents biases evolve quasi linearly with a greater increment for dry conditions. On the contrary, one can expect a more rapid limitation in temperature decrease with wet conditions, when soil reaches field capacity or saturation. The consequence on evapotranspiration deviation from reference clearly shows that beyond the [-10 % – +10 %] interval for water content biases, the error increases also linearly with a greater increment for dry conditions. Under -20 % bias, the impact on LE flux exceeds 50 Wm^{-2}. This result is important for our purpose to spatialize models for evapotranspiration estimates, because accurate root zone and surface water content retrievals from thermal and microwave remote sensing are a real challenge over heterogeneous landscapes (Barrett and Renzullo, 2009; Hain et al., 2011). The shift in temperature simulated by SEtHyS for -50 to +50 % water contents biases does not exceed 2 K and lay therefore within the typical remotely sensed surface temperature uncertainty range. For such a temperature bias, the TSEB model evapotranspiration divergence is lower than 40 Wm^{-2}. As a consequence, compared to the SEtHyS model, TSEB is less "reactive" to soil water contents variation. The result is critical for dry or stress conditions as previously pointed out. Actually, water status is only taken into account in the TSEB model through the surface temperature which is not sufficient and no additional limitation of surface evapotranspiration is done by modulating for instance the Priestley Taylor parameter.

4 Discussion

4.1 Influence of the parameters sets for model spatialization

The four calibration cases for the SEtHyS model going from site and period specific to more generic parameters from the literature are considered in order to evaluate the potential loss of model performance when specific calibration is not possible

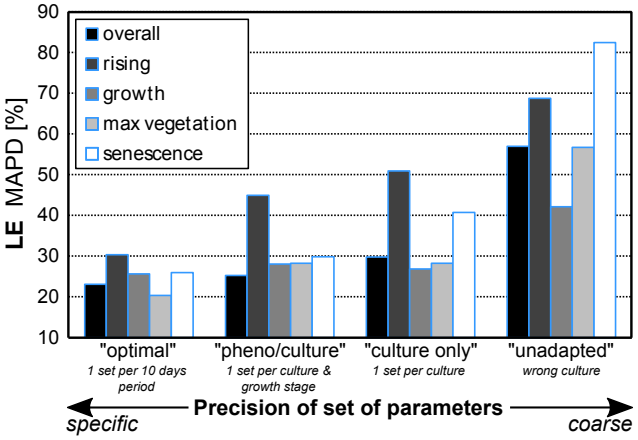

Figure 9. Impact of precision of sets of parameters on simulated fluxes; "optimal": most accurate per 10days period, "pheno+culture.": per culture and phase of growth as used for spatialization, "culture only": per culture (when only soil occupancy is known), "unadapted": incoherent (wrong culture).

by lack of data. Figure 6 shows the impact of the parameters set used on the SEtHyS performance to predict LE fluxes. Global results (for all crop classes and the whole cultural cycles) corresponding to the label "*overview*" in Fig. 6 give a MAPD of 30 % for the generic "*culture only*" set of parameters. This result does not differ much from the performance obtained with more specific sets of parameters "*pheno+cult*" or *"optimal"* giving 25 % and 23 % of MAPD, respectively. However, when a set of parameters from another crop class is used, MAPD reaches 58 %. A finest analysis by phenological stages indicates an overall stability of the results with the "*pheno+cult*" parameters set with regards to "*culture only*". There are actually two exceptions: one for the vegetation senescence periods which require specifics parameters sets. A mean set of parameters for the crop class increases MAPD from 30 % to 40 %. The second relates to crop rising periods. A generic one based only on the crop class ("*culture only*") increases MAPD up to 50 % compared to 45 % for "*pheno+cult*" when taking into account the phenology. As a conclusion, a mean parameters set associated to a specific crop without considering phenology implies only a slight decrease of the performance for growth or maximum vegetation development. By contrast, the relevance of the parameters sets becomes noticeable when specific information is not available for rising and senescence periods (including potentially water stress phases). With the same purpose, a specific analysis is dedicated to the Priestley-Taylor α_{PT} key parameter of the TSEB model in the next section.

4.2 A deeper look at the α_{PT} parameter for spatialization

A first estimation of $LE_{vegetation}$ canopy transpiration flux is obtained from the Priestley-Taylor approximation and depends on the fraction of green f_g and on the α_{PT} parameter. Most studies (Norman et al., 1995; Kustas and Norman, 1999; French et al., 2003; Anderson et al., 1997, 2008; Li et al., 2006, 2008, among others) have usually used a α_{PT} value of about 1.3 for semiarid or sub-humid agricultural areas. However, this value may vary with vegetation type as mentioned in Norman et al.

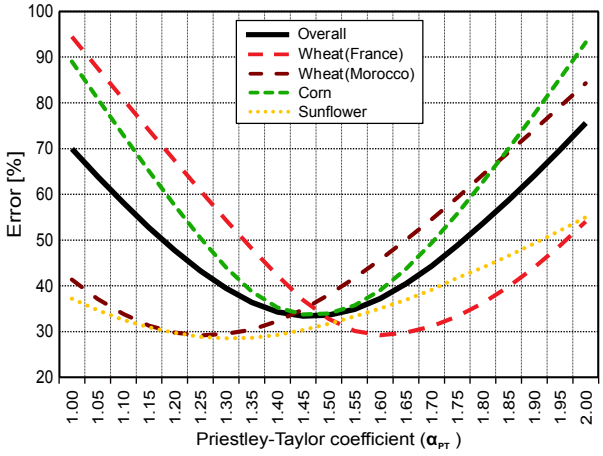

Figure 10. Sensitivity analyses of α_{PT} TSEB parameter during vegetation periods. Error was computed as a cost function (euclidian distance) taking into account MAPD of LE and H simultaneously: $Error = \sqrt{MAPD^2_{[LE]} + MAPD^2_{[H]}}$.

(1995), low values of LAI, atmospheric demand (Anderson et al., 2008; Agam et al., 2010; Colaizzi et al., 2014) or dry air advection conditions (Kustas and Norman, 1999). As a first step, the calibration is performed for midday time interval series over various surface and atmospheric conditions in order to be compared with previous studies using TSEB instantaneously for water flux mapping purpose when thermal imagery is available. Figure 10 shows the influence of α_{PT} values on H and LE fluxes for wheat, corn and sunflower crops over the sites in both the South West of France and Morocco. Optimal values for irrigated wheat in Morocco (semi-arid climate) and sunflower in the South-West of France (temperate climate) are close to the 1.3 bibliographical value. For wheat and irrigated corn in South-West of France, mean optimal values are higher and reach 1.6 for wheat. Mean optimal value of 1.5 is obtained for temperate climate, while a lower value of 1.25 is obtained for semi-arid climate. In a second step, the half-hourly data are used for the calibration in order to study the diurnal cycle of the α_{PT} parameter. The α_{PT} parameter shows a U-shape diurnal cycle evolution as displayed in Fig. 11 with smaller values around midday time, and higher values in both morning and evening when stability conditions are changing, enhancing $LE_{vegetation}$ transpiration canopy flux. This is particularly outlined under clear sky conditions, when TIR data from space is most likely to be collected. The original α_{PT} parameter is defined for a system at equilibrium with constant temperature, a condition which is particularly not met in the morning and in the evening when temperature temporal gradients are the highest. As a consequence, such variations integrated over the diurnal cycle lead to slightly higher α_{PT} fixed optimal values for daily half-hourly time interval simulations. Moreover, results indicate a decrease of RMSE by about 10 $\%$ on both H and LE fluxes when optimal values at the original time interval are used instead of a fixed daily average. Nevertheless, as more error on fluxes estimation is likely to occur around midday time, when turbulent fluxes are maximal, optimal daily value of α_{PT} tends towards its value around midday and is not much affected by increased morning and evening values. Despite thermal imagery from space is not available with the presence of clouds, the emergence of drone acquisition (Hoffmann et al., 2016) makes the characterization

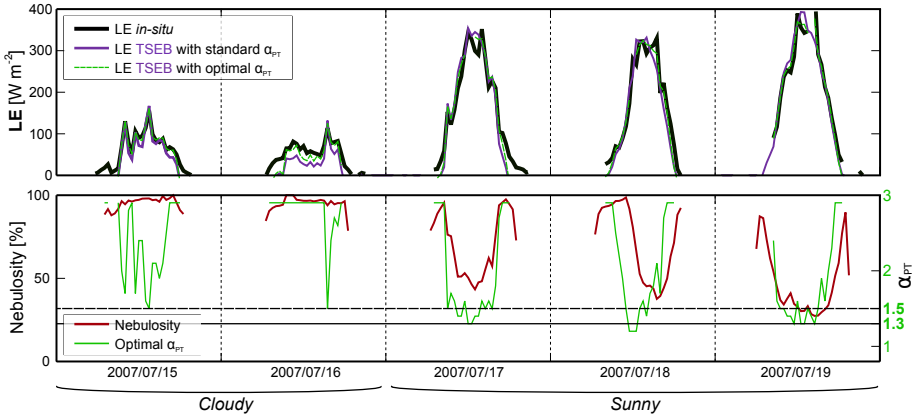

Figure 11. Influence of using optimal α_{PT} or averaged α_{PT} on LE estimates by TSEB, and influence of nebulosity on optimal α_{PT} estimates. Nebulosity was computed using Photosynthetically Active Radiation (PAR) measurements: $Nebulosity = \frac{PAR_{[diffuse]}}{PAR_{[total]}}$. Sample from Auradé 2007 sunflower plot.

of α_{PT} under those conditions of special interest. On cloudy days, Fig. 11 hilights that fixed daily optimal values of 1.8 to 2 (higher instantaneously) are required for optimizing H and LE fluxes enhancing again the $LE_{vegetation}$ transpiration flux for such reduced atmospheric demand. Hence, for simulation under cloudy conditions, α_{PT} value can be raised by +0.4 in a view to interpolate time series between satellite overpass or to run TSEB model with *in situ* or low altitude aircraft remotely sensed surface temperature. An improvement of about 10 % on LE flux simulation is likely to be expected when taking into account the above-mentioned impact of vegetation and cloudy conditions considerations on α_{PT} parameter retrieval. However, Colaizzi et al. (2014) remembered that larger α_{PT} values did not mitigate the discrepancies on the evaporation (E) and transpiration (T) components of the total latent heat flux (ET). These authors have proposed a revised version of TSEB replacing the Priestley-Taylor formulation with the Penman-Monteith equation in order to better account for large variations of vapor water pressure deficits and correct the evaporation, transpiration and total LE simulations. Boulet et al. (2015), thus built the SPARSE model based on Penman-Monteith with satisfying performances with the Morocco wheat site data set, above those of TSEB with default parameter values.

5 Summary and conclusions

Monitoring evapotranspiration at field scale over a large agricultural landscape is a challenge as it requires detailed information about surface state and meteorological forcing, which is prone to uncertainties and unavailability. This study aimed at evaluating the ability of a SVAT model (SEtHyS, described in Coudert et al., 2006) and an instantaneous energy balance model (TSEB, described in Norman et al., 1995) for mapping evapotranspiration over agricultural landscapes as a preliminary step to a joint use of both approaches through data assimilation as first proposed by Crow et al. (2005, 2008). Within this context, our specific objectives were: (1) to assess the skills and domains of validity of both modelling approaches at field scale for various

crop conditions, (2) to characterize model errors resulting from realistic uncertainties on inputs that can be expected from an application at the landscape scale. To this objective, this study takes advantage of a large and unique in situ database spanning two climates and seven different crop cycles. Main results drawn from this study can be summarized as follows:

- On average on the entire database, both models provide close statistical metrics on daily average values of LE (RMSEs of 36 Wm^{-2} for SEtHyS vs 39 Wm^{-2} for TSEB) while TSEB is slightly better on H predictions (21 vs 29 Wm^{-2}). This points out the remarkable performance of the TSEB model compared to the relative simplicity of the approach, all the more given that SEtHyS parameters are calibrated for each crop, each phenological stage and each site.

- SEtHyS skills appear more stable regardless of growth stages and crops whilst limitations of the TSEB model are clearly emphasized during rising and senescence stages.

- SEtHyS simulations of LE are less sensitive to noisy meteorological inputs than TSEB, for which performances are significantly deteriorated particularly when incoming radiation inputs are uncertain. Indeed, the partition between latent and sensible fluxes is moderated by the slow-varying soil moisture content in SEtHyS, while the TSEB partition relies on instantaneous measurement of available energy and surface temperature input only.

- The sensitivity analysis of surface temperature which is one of the more important inputs for TSEB shows that for a limited white noise up to 2 K, the drop of TSEB skills is small on both H and LE. By contrast, biases are much more impacting as a negative bias of 3 K could deteriorate LE RMSE from 58 Wm^{-2} to 78 Wm^{-2}.

- Similarly, the sensitivity of SEtHyS skills to uncertain water inputs and initial soil water content has also been analyzed and showed that emphasis should be put on water amount retrieval whilst timing of water supply appears of secondary importance; in particular a 10 mm negative bias on input coupled to a negatively biased initial SWC of 10 $\%$ with the same level, lead to a the loss of model performance above 25 $\%$.

- A cross sensitivity analysis of the TSEB and SEtHyS models to surface water status was carried out by simulating several surface temperature time series with SEtHyS and biased soil water contents (+/-10, +/-30 or +/-50 $\%$). The difference of surface temperature compared to a reference simulation is added as input to the TSEB model as an equivalent water bias converted in temperature. The shift in temperature simulated by SEtHyS for -50 to 50 $\%$ water contents biases does not exceed 2 K and is therefore within the typical remotely sensed surface temperature uncertainty range. For such a temperature bias, the TSEB model evapotranspiration divergence is lower than 20 Wm^{-2} while it reaches 50 Wm^{-2} for SEtHyS, which indicates that TSEB is less "reactive" to soil water contents variations than the SEtHyS model.

- Still with the scope to anticipate uncertainties induced by spatial distribution, SEtHyS was run with various sets of parameters of decreasing accuracies regarding the phenological stage and type of culture. This showed that when no precise information is known about surface condition, a valuable tradeoff is to consider a set of parameter only representative of the type of crop, provided vegetation is sufficiently developped. By contrast, the relevance of the parameters sets

becomes noticeable when specific information is not available for rising and senescence periods (including potentially water stress periods).

- For TSEB, an in-depth study of the Priestley-Taylor parameter α_{PT} hilighted optimal values of 1.8 to 2 under cloudy conditions, which is of particular interest with the emergence of low altitude drone acquisition, while most studies focus on clear-sky conditons when TIR aquisition from space is possible.

In addition to the characterization of the model and background errors, this study provided some insights to guide the implementation of a data assimilation algorithm at the scale of an agricultural landscape for the joint use of both approaches by highlighting deficiencies in specific conditions. Nevertheless, our current database suffer from a lack of hydric stress conditions and doesn't allow to characterise precisely this crucial aspect. A new experiment in Morocco (seasons 2017-2018 and 2018-2019) focusing on water stress on wheat field is currently being carried out. Our perspectives will focus on the exploitation of TIR data, by using TSEB as a proxy to be assimilated in SEtHyS following Crow et al. (2008), but also by taking advantage of the MCIP methodology to tune parameters to better fit surface temperature measurements following Coudert et al. (2008). Special consideration will be given to diurnal dynamics and to exploitation of relative differences inside plots and inter-plots.

Data availability. Data access from the French and the Moroccan sites must be requested to the head of the Sud-Ouest observatory (Tiphaine Tallec, CESBIO, France) and to the head of the TENSIFT observatory (Jamal Ezzahar, UCAM, Morocco). The SAFRAN data should be directly requested to the head of Météo-France (Toulouse, France).

Competing interests. The authors declare that they have no conflict of interest.

Acknowledgements. The authors wish to acknowledge the French Ministry of Research for funding the PhD scholarship of Guillaume Bigeard as well as USGS, NASA and JPL for providing LANDSAT and ASTER thermal Infrared data. This work was also partly supported by the French PNTS and TOSCA programs (with the "Assimilation multicritère dans la modélisation TSVA: complémentarité des grands domains spectraux" PNTS project by J. Demarty, the "Validité des estimations d'évapotranspiration basées sur l'utilisation de données infrarouges thermiques" PNTS project by D. Courault and the EVA2-IRT TOSCA project by G. Boulet and A. Olioso), the Seventh Framework Programme (FP7) with the SIRIUS project, the MISTRALS ENVIMED and SICMED programs and the Joint International Laboratory TREMA (http://trema.ucam.ac.ma) which allows collaborating with UCAM University for the application of the models on the Morocco site. The development of our methodologies is performed within the frame of the future TRISHNA mission of the French space agency (CNES) and the Indian Space Research Organization (ISRO). Finally, the authors would like to thank M. Anderson and W. Kustas from USDA-ARS for the dissemination of the TSEB model through the community which allows such research.

Appendix A: SEtHyS main equations

This section presents the governing equations for the SEtHyS SVAT model variables.

A1 Basical set of equations for the SEtHyS model

The mass and energy budget is solved jointly for both soil and vegetation sources from the following system:

$$\begin{cases} R_{n[soil]} = H_{[soil]} + LE_{[soil]} + G \\ R_{n[veg]} = H_{[veg]} + LE_{[veg]} \\ H = H_{[veg]} + H_{[soil]} \\ E = E_{[veg]} + E_{[soil]}, \end{cases} \tag{A1}$$

where $R_{n[soil]}$ and $R_{n[veg]}$ are net radiations at soil and vegetation levels and G is the soil heat flux. Parameterization of the soil behavior is based on Deardorff's formalism (1978). The soil surface temperature $T_{[soil]}$, the vegetation temperature $T_{[veg]}$, the air temperature inside the canopy $T_{[canopy]}$ and the air humidity inside the canopy $q_{[canopy]}$ are determined by a first order linearization of the previous equations system.

The soil surface temperature method prediction is namely the force restore method (Bhumralkar, 1975; Blackadar, 1976) and requires deep soil temperature T_2. T_2 can be estimated from the mean air temperature over the 24 previous hours for short-range studies (Blackadar, 1976). The heat capacity is prescribed by de Vries's model (1963) and hydrodynamic properties result from pedotransfer functions (retention curve, hydraulic conductivity) based on Genuchten's approach (1980) under Mualem hypothesis (1976).

Prognostic equation for ground surface temperature is written as:

$$\frac{\partial T_{[soil]}}{\partial t} = \frac{2\sqrt{\pi}}{C_e}(R_n - H - LE) - \frac{2\pi}{\tau}\left(T_{[soil]} - T_2\right). \tag{A2}$$

The factor C_e is an equivalent heat capacity related to the diurnal thermal wave damping layer. In SEtHyS, the parameterization of the equivalent heat capacity has been weighted by introducing an empirical factor (F_{therm} in parameters list, Table 2) compared to Deardorff (1978).

Deardorff (1978) proposed a similar approach of ground soil moisture, leading to the following equations:

$$\begin{aligned} \frac{\partial w_g}{\partial t} &= -\frac{E_g + 0.2E_v\left(\frac{w_g}{w_{\max}}\right) - P}{dp_1} \\ &\quad - C\left(w_g, w_2\right)\left(w_g - w_2\right) \end{aligned} \tag{A3}$$

$$\frac{\partial w_2}{\partial t} = -\frac{E_g + E_v - P}{dp_2}, \tag{A4}$$

where $w_{\max}$ is the soil moisture at soil saturation, w_g and w_2 are surface and root zone water contents, P is the precipitation rate, dp_1 and dp_2 are the surface and root zone layers depths.

A2 Radiative budget

Incoming radiation partition for optical (VIS) and infrared (IR) wavelength is performed through a shielding factor σ_f tighly linked to vegetation density. Its expression is as follows by considering a spherical distribution of leaves (François, 2002) with the hypothesis of diffuse radiation for longwave domain and direct vertical radiation in shortwave domain:

$$\begin{cases} \sigma_f = 1 - e^{-0.825LAI} & \text{for longwave domain} \\ \sigma_f = 1 - e^{-0.5LAI} & \text{for shortwave domain} \end{cases} \tag{A5}$$

Radiative budget is then solved jointly at the soil and at the vegetation level for short and long wavelengths. Concerning short wavelengths, soil albedo α_{soil} is linearly linked to surface soil moisture. Vegetation albedo α_{veg} is a model parameter. The net radiation for the soil $R_{n[soil],SW}$ and for the vegetation $R_{n[veg],SW}$ are as follow ("Mod3" parameterization as proposed in François, 2002):

$$R_{n[soil],SW} = S^{\downarrow} \frac{(1-\sigma_f)(1-\alpha_{soil})}{1-\sigma_f \alpha_{veg} \alpha_{soil}}, \tag{A6}$$

and at canopy level:

$$R_{n[veg],SW} = S^{\downarrow}(1-\alpha_{veg})\sigma_f \left[1 + \alpha_{soil} \frac{(1-\sigma_f)}{1-\sigma_f \alpha_{soil} \alpha_{veg}}\right] \tag{A7}$$

where $S^{\downarrow}$ is the incoming shortwave radiation.

Concerning long wavelengths, the net radiation for soil $R_{n[soil],LW}$ and vegetation $R_{n[veg],LW}$ are given by:

$$\begin{aligned} R_{n[soil],LW} = {} & (1-\sigma_f) \frac{\varepsilon_g (R_a^{\downarrow} - \sigma T_{[soil]}^4)}{1-\sigma_f(1-\varepsilon_f)(1-\varepsilon_g)} \\ & - \frac{\varepsilon_g \varepsilon_f \sigma_f \sigma (T_{[soil]}^4 - T_{[veg]}^4)}{1-\sigma_f(1-\varepsilon_f)(1-\varepsilon_g)} \end{aligned} \tag{A8}$$

$$\begin{aligned} R_{n[veg],LW} = {} & \sigma_f \left[\varepsilon_f (R_a^{\downarrow} - \sigma T_f^4) + \frac{\varepsilon_g \varepsilon_f \sigma (T_{[soil]}^4 - T_{[veg]}^4)}{1-\sigma_f(1-\varepsilon_f)(1-\varepsilon_g)}\right] \\ & + \sigma_f \frac{(1-\varepsilon_f)(1-\varepsilon_g)\varepsilon_f (R_a^{\downarrow} - \sigma T_{[veg]}^4)}{1-\sigma_f(1-\varepsilon_f)(1-\varepsilon_g)} \end{aligned} \tag{A9}$$

Direct solar shortwave radiation $S^{\downarrow}$ and atmospheric longwave radiation $R^{\downarrow}$ are input model data.
The thermal infrared surface temperature T_B (observed above the canopy) results from the partitioning of the surface and the radiative interaction between soil (whose temperature is $T_{[soil]}$) and the vegetation above (whose temperature is $T_{[veg]}$).

A3 Heat fluxes expressions

The mass and energy transfers in equilibrium with net surface radiation are momentum, sensible and latent heat fluxes. A conductance formalism allows expressing them by considering the canopy as a single vegetation layer (at some height Z_{af}) above ground (Thom, 1972). Thus, following the electrical (Ohm's law) analogy, soil surface, leaves surface, air canopy space and atmosphere above canopy are the levels between which differences of potential (temperature and humidity gradients) and transfer coefficients *i.e.* aerodynamic conductances can be calculated.
Heat fluxes H and LE (sensible and latent heat fluxes respectively) are then determined at three levels:
at atmospheric reference level,

$$H = \rho c_p C_h \left(T_{[canopy]} - T_a\right) \tag{A10}$$

$$LE = \frac{\rho c_p}{\gamma} C_h \left(q_{[canopy]} - q_a\right) \tag{A11}$$

at vegetation level,

$$H_{[veg]} = \rho c_p C_{h[veg]} \left(T_{[veg]} - T_{[canopy]}\right) \tag{A12}$$

$$LE_{[veg]} = \frac{\rho c_p}{\gamma} C_{h[veg]} R' \left(q_{sat}(T_{[veg]}) - q_{[canopy]}\right) \tag{A13}$$

and at ground level,

$$H_{[soil]} = \rho c_p C_{h[soil]} \left(T_{[soil]} - T_{[canopy]}\right) \tag{A14}$$

$$LE_{[soil]} = \frac{\rho c_p}{\gamma} C_{h[soil]} C_s \left(q_{sat}(T_{[soil]}) - q_{[canopy]}\right) \tag{A15}$$

with

$$LE = LE_{[soil]} + LE_{[veg]} \tag{A16}$$

$$H = H_{[soil]} + H_{[veg]} \tag{A17}$$

and G conduction heat flux in soil is residual of the energy budget :

$$G = R_{n[soil],LW} + R_{n[soil],SW} - H_{[soil]} \breve{} LE_{[soil]} \tag{A18}$$

where C_p is the specific heat at constant pressure, γ is the psychrometric constant, T, q are temperature and water vapor pressure and a, g, $canopy$ are indices relative to air, ground, and canopy air space.

C_h, $C_{h[veg]}$ and $C_{h[soil]}$ are respectively aerodynamic conductances between canopy air space and the overlaying atmosphere, leaves surface and canopy air space, ground and canopy air space, $R^{'}$ factor is defined below. These variables are derived from the eddy fluxes theory between two atmospheric levels. In SEtHyS model, the formulation follows the parameterization proposed by Shuttleworth and Wallace (1985) with a constant extinction coefficient in the exponential wind speed profile.

C_s is the ground evaporation conductance; it depends on soil moisture conditions and potential evaporation $E_{pot[soil]}$ (Bernard et al., 1986; Wetzel and Chang, 1988; Soares et al., 1988):

$$C_s = \min\left(1, \frac{E_{\lim}}{E_{pot[soil]}}\right), \tag{A19}$$

where E_{lim} depends on soil properties (composition and moisture), Soares et al. (1988) gives the expression:

$$E_{\lim} = a_{Elim}\left(\exp(b_{Elim}(w_g - w_{resid})^2) - 1\right) \tag{A20}$$

a_{Elim} and b_{Elim} are model parameters related to soil evaporation response.

$R^{'}$ factor in Eq.(A13) accounts for stomatal resistance and to the fact that only the fraction of the canopy area which is not covered by water will contribute to evapotranspiration. Deardorff (1978) proposed the expression:

$$R^{'} = \left(\frac{dew}{d_{\max}}\right)^{2/3} + \left[1 - \left(\frac{dew}{d_{\max}}\right)^{2/3}\right] \frac{1}{(\beta + C_{fh} RST)}, \tag{A21}$$

$R^{'} = 1$ for condensation,

where "dew" (resp. "d_{max}") is the fraction (resp. the maximal one) of free water on the foliage. RST is the stomatal resistance, this factor governs the canopy participation to the energy budget and is responsible for partition between sensible and latent heat fluxes.

In the model, calculation of RST is based on Collatz et al. (1991, 1992) and is the same as in SiB models (Sellers et al., 1992, 1996). Biophysical and environmental variables manage photosynthesis processes giving CO_2 assimilation rate and then stomatal conductance of the foliage.

Ball (1988) gives the following leaf stomatal conductance expression:

$$g_s = m\frac{A_n}{c_s}h_s p + b \tag{A22}$$

where A_n is net assimilation rate calculated by the model of Farquhar et al. (1980), c_s and h_s are CO_2 partial pressure and relative humidity at leaf surface, p is atmospheric pressure, m and b are empirical factors from observations depending on vegetation type (C_3 or C_4).

Assimilation rate is determined by means of three factors, a photosynthetic enzyme (Rubisco) limiting rate, a light limiting rate and a limiting rate owing to the leaf capacity to export or utilize the photosynthesis products (Collatz et al., 1991). In the model, the iterative solution method for the photosynthesis-stomatal conductance calculation proposed by Collatz et al. (1991) has been implemented. Indeed, canopy is considered as a "big leaf" assuming bulk or integral values over canopy depth used in the integrated form of Eq.(A22) (see Sellers et al., 1992). Stomatal conductance and net assimilation rate are then determined for the canopy.

References

Agam, N., Kustas, W. P., Anderson, M. C., Norman, J. M., Colaizzi, P. D., Howell, T. A., Prueger, J. H., Meyers, T. P., and Wilson, T. B.: Application of the Priestley–Taylor Approach in a Two-Source Surface Energy Balance Model, Journal of Hydrometeorology, 11, 185–198, https://doi.org/10.1175/2009JHM1124.1, http://journals.ametsoc.org/doi/abs/10.1175/2009JHM1124.1, 2010.

Allen, R. G., Pereira, L. S., Raes, D., and Smith, M.: Crop evapotranspiration-Guidelines for computing crop water requirements-FAO Irrigation and drainage paper 56, FAO, Rome, pp. 1–15, http://www.engr.scu.edu/~emaurer/classes/ceng140_watres/handouts/FAO_56_Evapotranspiration.pdf, 1998.

Allen, R. G., Pereira, L. S., Howell, T. A., and Jensen, M. E.: Evapotranspiration information reporting: I. Factors governing measurement accuracy, Agricultural Water Management, 98, 899–920, https://doi.org/10.1016/j.agwat.2010.12.015, http://linkinghub.elsevier.com/retrieve/pii/S0378377411000023, 2011.

Anderson, M., Norman, J., and Diak, G.: A two-source time-integrated model for estimating surface fluxes using thermal infrared remote sensing, Remote Sensing of Environment, 60, 195–216, https://doi.org/10.1016/S0034-4257(96)00215-5, http://www.sciencedirect.com/science/article/pii/S0034425796002155http://linkinghub.elsevier.com/retrieve/pii/S0034425796002155, 1997.

Anderson, M. C., Norman, J. M., Kustas, W. P., Li, F., Prueger, J. H., and Mecikalski, J. R.: Effects of Vegetation Clumping on Two–Source Model Estimates of Surface Energy Fluxes from an Agricultural Landscape during SMACEX, Journal of Hydrometeorology, 6, 892–909, https://doi.org/10.1175/JHM465.1, http://journals.ametsoc.org/doi/abs/10.1175/JHM465.1, 2005.

Anderson, M. C., Norman, J. M., Mecikalski, J. R., Otkin, J. A., and Kustas, W. P.: A climatological study of evapotranspiration and moisture stress across the continental United States based on thermal remote sensing: 1. Model formulation, Journal of Geophysical Research, 112, D10 117, https://doi.org/10.1029/2006JD007506, http://www.agu.org/pubs/crossref/2007/2006JD007506.shtml, 2007.

Anderson, M. C., Norman, J. M., Kustas, W. P., Houborg, R., Starks, P., and Agam, N.: A thermal-based remote sensing technique for routine mapping of land-surface carbon, water and energy fluxes from field to regional scales, Remote Sensing of Environment, 112, 4227–4241, https://doi.org/10.1016/j.rse.2008.07.009, http://linkinghub.elsevier.com/retrieve/pii/S0034425708002289, 2008.

Aubinet, M., Grelle, A., Ibrom, A., Rannik, U., Moncrieff, J., Foken, T., Kowalski, A. S., Martin, P. H., Berbigier, P., Bernhofer, C., Clement, R., Elbers, J., Granier, A., Grunwald, T., Morgenstern, K., Pilegaard, K., Rebmann, C., Snijders, W., Valentini, R., and Vesala, T.: Estimates of the annual net carbon and water exchange of forests: The EUROFLUX methodology, Advances In Ecological Research, 30, 113–175, https://doi.org/10.1016/S0065-2504(08)60018-5, http://www.sciencedirect.com/science/article/B7CT4-4S9FXK6-7/2/58452452609b17bb0c0af17c132209f9, 2000.

Ball, J.: An analysis of stomatal conductance, Ph.D. thesis, Stanford, http://dge.stanford.edu/publications/berry/AnnRev2012/1988Ball.pdf, 1988.

Barrett, D. J. and Renzullo, L. J.: On the Efficacy of Combining Thermal and Microwave Satellite Data as Observational Constraints for Root-Zone Soil Moisture Estimation, Journal of Hydrometeorology, 10, 1109–1127, https://doi.org/10.1175/2009JHM1043.1, http://journals.ametsoc.org/doi/abs/10.1175/2009JHM1043.1, 2009.

Becker, F. and Li, Z.-L.: Temperature-independent spectral indices in thermal infrared bands, Remote Sensing of Environment, 32, 17–33, https://doi.org/10.1016/0034-4257(90)90095-4, http://linkinghub.elsevier.com/retrieve/pii/0034425790900954, 1990.

Becker, F. and Li, Z. L.: Surface temperature and emissivity at various scales: Definition, measurement and related problems, Remote Sensing Reviews, 12, 225–253, https://doi.org/10.1080/02757259509532286, http://www.tandfonline.com/doi/abs/10.1080/02757259509532286, 1995.

Bernard, R., Soares, J. V., and Vidal-Madjar, D.: Differential Bare Field Drainage Properties From Airborne Microwave Observations, Water Resources Research, 22, 869–875, https://doi.org/10.1029/WR022i006p00869, http://doi.wiley.com/10.1029/WR022i006p00869, 1986.

Béziat, P., Ceschia, E., and Dedieu, G.: Carbon balance of a three crop succession over two cropland sites in South West France, Agricultural and Forest Meteorology, 149, 1628–1645, https://doi.org/10.1016/j.agrformet.2009.05.004, http://linkinghub.elsevier.com/retrieve/pii/S016819230900118X, 2009.

Bhumralkar, C. M.: Numerical Experiments on the Computation of Ground Surface Temperature in an Atmospheric General Circulation Model, Journal of Applied Meteorology, 14, 1246–1258, https://doi.org/10.1175/1520-0450(1975)014<1246:NEOTCO>2.0.CO;2, http://journals.ametsoc.org/doi/abs/10.1175/1520-0450(1975)014<1246:NEOTCO>2.0.CO;2, 1975.

Bigeard, G.: Estimation spatialisée de l'évapotranspiration à l'aide de données infra-rouge thermique multi-résolutions., Ph.D. thesis, University of Toulouse, 2014.

Blackadar, A.: Modeling the nocturnal boundary layer, in: Proceedings of the Third Symposium on Atmospheric Turbulence, Diffusion and Air Quality., Proceedings of the Third Symposium on Atmospheric Turbulence, Diffusion and Air Quality, pp. 46–49, American Meteorological Society, Raleigh, 1976.

Boulet, G., Chehbouni, A., Gentine, P., Duchemin, B., Ezzahar, J., and Hadria, R.: Monitoring water stress using time series of observed to unstressed surface temperature difference, Agricultural and Forest Meteorology, 146, 159–172, https://doi.org/10.1016/j.agrformet.2007.05.012, http://linkinghub.elsevier.com/retrieve/pii/S0168192307001487, 2007.

Boulet, G., Mougenot, B., Lhomme, J.-P., Fanise, P., Lili-Chabaane, Z., Olioso, A., Bahir, M., Rivalland, V., Jarlan, L., Merlin, O., Coudert, B., Er-Raki, S., and Lagouarde, J.-P.: The SPARSE model for the prediction of water stress and evapotranspiration components from thermal infra-red data and its evaluation over irrigated and rainfed wheat, Hydrology and Earth System Sciences, 19, 4653–4672, https://doi.org/10.5194/hess-19-4653-2015, https://www.hydrol-earth-syst-sci.net/19/4653/2015/, 2015.

Calvet, J.-C., Noilhan, J., Roujean, J.-L., Bessemoulin, P., Cabelguenne, M., Olioso, A., and Wigneron, J.-P.: An interactive vegetation SVAT model tested against data from six contrasting sites, Agricultural and Forest Meteorology, 92, 73–95, 1998.

Campbell, G. S. and Norman, J. M.: An introduction to environmental biophysics, Springer Science & Business Media, 1998.

Carlson, T.: An Overview of the "Triangle Method" for Estimating Surface Evapotranspiration and Soil Moisture from Satellite Imagery, Sensors, 7, 1612–1629, http://www.mdpi.com/1424-8220/7/8/1612, 2007.

Carrer, D., Lafont, S., Roujean, J.-L., Calvet, J.-C., Meurey, C., Le Moigne, P., and Trigo, I. F.: Incoming Solar and Infrared Radiation Derived from METEOSAT: Impact on the Modeled Land Water and Energy Budget over France, Journal of Hydrometeorology, 13, 504–520, https://doi.org/10.1175/JHM-D-11-059.1, http://journals.ametsoc.org/doi/abs/10.1175/JHM-D-11-059.1, 2012.

Chávez, J., Neale, C. M., Hipps, L. E., Prueger, J. H., and Kustas, W. P.: Comparing aircraft-based remotely sensed energy balance fluxes with eddy covariance tower data using heat flux source area functions, Journal of Hydrometeorology, 6, 923–940, 2005.

Chehbouni, A., Escadafal, R., Duchemin, B., Boulet, G., Simonneaux, V., Dedieu, G., Mougenot, B., Khabba, S., Kharrou, H., Maisongrande, P., Merlin, O., Chaponniere, A., Ezzahar, J., Er-Raki, S., Hoedjes, J., Hadria, R., Abourida, A., Cheggour, A., Raibi, F., Boudhar, A., Benhadj, I., Hanich, L., Benkaddour, A., Guemouria, N., Chehbouni, A., Lahrouni, A., Olioso, A., Jacob, F., Williams, D., and Sobrino, J.: An integrated modelling and remote sensing approach for hydrological study in arid and semi-arid regions: the SUDMED Programme, International Journal of Remote Sensing, 29, 5161–5181, https://doi.org/10.1080/01431160802036417, http://www.tandfonline.com/doi/abs/10.1080/01431160802036417, 2008.

Chirouze, J., Boulet, G., Jarlan, L., Fieuzal, R., Rodriguez, J. C., Ezzahar, J., Er-Raki, S., Bigeard, G., Merlin, O., Garatuza-Payan, J., Watts, C., and Chehbouni, G.: Intercomparison of four remote-sensing-based energy balance methods to retrieve surface evapotranspiration and

water stress of irrigated fields in semi-arid climate, Hydrology and Earth System Sciences, 18, 1165–1188, https://doi.org/10.5194/hess-18-1165-2014, http://www.hydrol-earth-syst-sci.net/18/1165/2014/, 2014.

Choi, M., Kustas, W. P., Anderson, M. C., Allen, R. G., Li, F., and Kjaersgaard, J. H.: An intercomparison of three remote sensing-based surface energy balance algorithms over a corn and soybean production region (Iowa, U.S.) during SMACEX, Agricultural and Forest Meteorology, 149, 2082–2097, https://doi.org/10.1016/j.agrformet.2009.07.002, http://linkinghub.elsevier.com/retrieve/pii/S0168192309001671, 2009.

Choudhury, B., Idso, S., and Reginato, R.: Analysis of an empirical model for soil heat flux under a growing wheat crop for estimating evaporation by an infrared-temperature based energy balance equation, Agricultural and Forest Meteorology, 39, 283–297, https://doi.org/10.1016/0168-1923(87)90021-9, http://linkinghub.elsevier.com/retrieve/pii/0168192387900219, 1987.

Claverie, M.: Estimation spatialisée de la biomasse et des besoins en eau des cultures à l'aide de données satellitales à hautes résolutions spatiale et temporelle : application aux agrosystèmes du sud-ouest de la France., Ph.D. thesis, University of Toulouse, 2011.

Claverie, M., Demarez, V., Duchemin, B., Hagolle, O., Ducrot, D., Marais-Sicre, C., Dejoux, J.-F., Huc, M., Keravec, P., Béziat, P., Fieuzal, R., Ceschia, E., and Dedieu, G.: Maize and sunflower biomass estimation in southwest France using high spatial and temporal resolution remote sensing data, Remote Sensing of Environment, 124, 844–857, https://doi.org/10.1016/j.rse.2012.04.005, http://linkinghub.elsevier.com/retrieve/pii/S0034425712001678, 2012.

Colaizzi, P. D., Kustas, W. P., Anderson, M. C., Agam, N., Tolk, J. A., Evett, S. R., Howell, T. A., Gowda, P. H., and O'Shaughnessy, S. A.: Two-source energy balance model estimates of evapotranspiration using component and composite surface temperatures, Advances in Water Resources, 50, 134–151, https://doi.org/10.1016/j.advwatres.2012.06.004, http://linkinghub.elsevier.com/retrieve/pii/S0309170812001546, 2012.

Colaizzi, P. D., Agam, N., Tolk, J. A., Evett, S. R., Howell, T. A., Gowda, P. H., O'Shaughnessy, S. A., Kustas, W. P., and Anderson, M. C.: Two-source energy balance model to calculate E, T, and ET: Comparison of Priestley-Taylor and Penman-Monteith formulations and two time scaling methods, Transactions of the ASABE, 57, 479–498, 2014.

Collatz, G., Ball, J., Grivet, C., and Berry, J.: Physiological and environmental regulation of stomatal conductance, photosynthesis and transpiration: a model that includes a laminar boundary layer, Agricultural and Forest Meteorology, 54, 107–136, https://doi.org/10.1016/0168-1923(91)90002-8, http://www.sciencedirect.com/science/article/pii/0168192391900028, 1991.

Collatz, G., Ribas-Carbo, M., and Berry, J.: Coupled Photosynthesis-Stomatal Conductance Model for Leaves of C4 Plants, Australian Journal of Plant Physiology, 19, 519, https://doi.org/10.1071/PP9920519, http://www.publish.csiro.au/?paper=PP9920519, 1992.

Coudert, B. and Ottlé, C.: An improved SVAT model calibration strategy based on the optimisation of surface temperature temporal dynamics, Geophysical Research Letters, 34, 1–6, https://doi.org/10.1029/2006GL028778, http://www.agu.org/pubs/crossref/2007/2006GL028778.shtml, 2007.

Coudert, B., Ottlé, C., Boudevillain, B., Demarty, J., and Guillevic, P.: Contribution of Thermal Infrared Remote Sensing Data in Multiobjective Calibration of a Dual-Source SVAT Model, Journal of Hydrometeorology, 7, 404–420, https://doi.org/10.1175/JHM503.1, http://journals.ametsoc.org/doi/abs/10.1175/JHM503.1, 2006.

Coudert, B., Ottlé, C., and Briottet, X.: Monitoring land surface processes with thermal infrared data: Calibration of SVAT parameters based on the optimisation of diurnal surface temperature cycling features, Remote Sensing of Environment, 112, 872–887, https://doi.org/10.1016/j.rse.2007.06.024, http://linkinghub.elsevier.com/retrieve/pii/S0034425707003926, 2008.

Courault, D., Seguin, B., and Olioso, A.: Review on estimation of evapotranspiration from remote sensing data: From empirical to numerical modeling approaches, Irrigation and Drainage Systems, 19, 223–249, https://doi.org/10.1007/s10795-005-5186-0, http://www.springerlink.com/index/10.1007/s10795-005-5186-0, 2005.

Crow, W. T., Li, F., and Kustas, W. P.: Intercomparison of spatially distributed models for predicting surface energy flux patterns during SMACEX, Journal of hydrometeorology, 6, 941–953, http://journals.ametsoc.org/doi/pdf/10.1175/JHM468.1, 2005.

Crow, W. T., Kustas, W. P., and Prueger, J. H.: Monitoring root-zone soil moisture through the assimilation of a thermal remote sensing-based soil moisture proxy into a water balance model, Remote Sensing of Environment, 112, 1268–1281, https://doi.org/10.1016/j.rse.2006.11.033, http://linkinghub.elsevier.com/retrieve/pii/S0034425707003252, 2008.

de Vries, D.: Thermal properties of soils, vol. 1, Amsterdam, New Holland, 382p, 1963.

Deardorff, J. W.: Efficient prediction of ground surface temperature and moisture, with inclusion of a layer of vegetation, Journal of Geophysical Research, 83, 1889, https://doi.org/10.1029/JC083iC04p01889, http://www.agu.org/pubs/crossref/1978/JC083iC04p01889.shtml, 1978.

Dedieu, G., Chehbouni, G., Demarez, V., Ducrot, D., Flouzat, G., Gastellu-Etchegorry, J., Gouaux, P., Lamaze, T., Lavenu, F., and Toan, T. L.: Carbon and water balance of France south-west region: An outline of the Sud-Ouest project., in: Physical measurements & signatures in remote sensing. International symposium, pp. 725–728, 2001.

Demarty, J., Ottlé, C., Braud, I., Olioso, A., Frangi, J., Bastidas, L., and Gupta, H.: Using a multiobjective approach to retrieve information on surface properties used in a SVAT model, Journal of Hydrology, 287, 214–236, https://doi.org/10.1016/j.jhydrol.2003.10.003, http://linkinghub.elsevier.com/retrieve/pii/S0022169403004177, 2004.

Demarty, J., Ottlé, C., Braud, I., Olioso, A., Frangi, J. P., Gupta, H. V., and Bastidas, L. A.: Constraining a physically based Soil-Vegetation-Atmosphere Transfer model with surface water content and thermal infrared brightness temperature measurements using a multiobjective approach, Water Resources Research, 41, W01 011, https://doi.org/10.1029/2004WR003695, http://www.agu.org/pubs/crossref/2005/2004WR003695.shtml, 2005.

Diarra, A., Jarlan, L., Er-Raki, S., Le Page, M., Khabba, S., Bigeard, G., Tavernier, A., Chirouze, J., Fanise, P., Moutamanni, A., et al.: Characterization of evapotranspiration over irrigated crops in a semi-arid area (Marrakech, Morocco) using an energy budget model, Procedia Environmental Sciences, 19, 504–513, 2013.

Diarra, A., Jarlan, L., Er-Raki, S., Le Page, M., Aouade, G., Tavernier, A., Boulet, G., Ezzahar, J., Merlin, O., and Khabba, S.: Performance of the two-source energy budget (TSEB) model for the monitoring of evapotranspiration over irrigated annual crops in North Africa, Agricultural Water Management, 193, 71–88, 2017.

Douville, H.: Validation and sensitivity of the global hydrologic budget in stand-alone simulations with the ISBA land-surface scheme, Climate Dynamics, 14, 151–172, https://doi.org/10.1007/s003820050215, http://www.springerlink.com/openurl.asp?genre=article&id=doi:10.1007/s003820050215, 1998.

Duchemin, B., Hadria, R., Erraki, S., Boulet, G., Maisongrande, P., Chehbouni, A., Escadafal, R., Ezzahar, J., Hoedjes, J., Kharrou, M., Khabba, S., Mougenot, B., Olioso, A., Rodriguez, J.-C., and Simonneaux, V.: Monitoring wheat phenology and irrigation in Central Morocco: On the use of relationships between evapotranspiration, crops coefficients, leaf area index and remotely-sensed vegetation indices, Agricultural Water Management, 79, 1–27, https://doi.org/10.1016/j.agwat.2005.02.013, http://linkinghub.elsevier.com/retrieve/pii/S0378377405001046, 2006.

Er-Raki, S., Chehbouni, A., Khabba, S., Simonneaux, V., Jarlan, L., Ouldbba, A., Rodriguez, J., and Allen, R.: Assessment of reference evapotranspiration methods in semi-arid regions: can weather forecast data be used as alternate of ground meteorological parameters?, Journal of Arid Environments, 74, 1587–1596, 2010.

Eugster, W., McFadden, J., and Chapin, F.: A comparative approach to regional variation in surface fluxes using mobile eddy correlation towers, Boundary-Layer Meteorology, pp. 293–307, http://www.springerlink.com/index/V83P5125Q4G68741.pdf, 1997.

Farquhar, G. D., Caemmerer, S., and Berry, J. A.: A biochemical model of photosynthetic CO2 assimilation in leaves of C3 species, Planta, 149, 78–90, https://doi.org/10.1007/BF00386231, http://link.springer.com/article/10.1007/BF00386231http://link.springer.com/10.1007/BF00386231, 1980.

François, C.: The potential of directional radiometric temperatures for monitoring soil and leaf temperature and soil moisture status, Remote Sensing of Environment, 80, 122–133, https://doi.org/10.1016/S0034-4257(01)00293-0, http://linkinghub.elsevier.com/retrieve/pii/S0034425701002930, 2002.

Franks, S., Beven, K. J., Quinn, P., and Wright, I.: On the sensitivity of soil-vegetation-atmosphere transfer (SVAT) schemes: equifinality and the problem of robust calibration, Agricultural and Forest Meteorology, 86, 63–75, 1997.

French, A. N., Schmugge, T. J., Kustas, W. P., Brubaker, K. L., and Prueger, J.: Surface energy fluxes over El Reno, Oklahoma, using high-resolution remotely sensed data, Water Resources Research, 39, n/a–n/a, https://doi.org/10.1029/2002WR001734, http://doi.wiley.com/10.1029/2002WR001734, 2003.

French, A. N., Jacob, F., Anderson, M. C., Kustas, W. P., Timmermans, W. J., Gieske, A., Su, Z., Su, H., McCabe, M. F., and Li, F.: Surface energy fluxes with the Advanced Spaceborne Thermal Emission and Reflection radiometer (ASTER) at the Iowa 2002 SMACEX site (USA), Remote Sensing of Environment, 99, 55–65, http://www.sciencedirect.com/science/article/B6V6V-4GP1VM2-3/2/8b4703da73ae386884eea21078865f92, 2005.

Genuchten, M. V.: A closed-form equation for predicting the hydraulic conductivity of unsaturated soils, Soil Science Society of America ..., 44, 892–898, https://dl.sciencesocieties.org/publications/sssaj/abstracts/44/5/SS0440050892, 1980.

Gillespie, A., Rokugawa, S., Matsunaga, T., Cothern, J., Hook, S., and Kahle, A.: A temperature and emissivity separation algorithm for Advanced Spaceborne Thermal Emission and Reflection Radiometer (ASTER) images, IEEE Transactions on Geoscience and Remote Sensing, 36, 1113–1126, https://doi.org/10.1109/36.700995, http://ieeexplore.ieee.org/lpdocs/epic03/wrapper.htm?arnumber=700995, 1998.

Hain, C. R., Crow, W. T., Mecikalski, J. R., Anderson, M. C., and Holmes, T.: An intercomparison of available soil moisture estimates from thermal infrared and passive microwave remote sensing and land surface modeling, Journal of Geophysical Research, 116, 1–18, https://doi.org/10.1029/2011JD015633, http://www.agu.org/pubs/crossref/2011/2011JD015633.shtml, 2011.

Hall, F. G., Huemmrich, K. F., Goetz, S. J., Sellers, P. J., and Nickeson, J. E.: Satellite remote sensing of surface energy balance - Success, failures, and unresolved issues in FIFE, Journal of Geophysical Research, 97, 19 061–19 089, http://www.agu.org/pubs/crossref/1992/92JD02189.shtml, 1992.

Hoffmann, H., Nieto, H., Jensen, R., Guzinski, R., Zarco-Tejada, P., and Friborg, T.: Estimating evaporation with thermal UAV data and two-source energy balance models, Hydrology and Earth System Sciences, 20, 697–713, https://doi.org/10.5194/hess-20-697-2016, https://www.hydrol-earth-syst-sci.net/20/697/2016/, 2016.

Hssaine, B. A., Merlin, O., Rafi, Z., Ezzahar, J., Jarlan, L., Khabba, S., and Er-Raki, S.: Calibrating an evapotranspiration model using radiometric surface temperature, vegetation cover fraction and near-surface soil moisture data, Agricultural and Forest Meteorology, 256, 104–115, 2018.

Jarlan, L., Khabba, S., Er-Raki, S., Page, M. L., Hanich, L., Fakir, Y., Merlin, O., Mangiarotti, S., Gascoin, S., Ezzahar, J., Kharrou, M., Berjamy, B., Saaïdi, A., Boudhar, A., Benkaddour, A., Laftouhi, N., Abaoui, J., Tavernier, A., Boulet, G., Simonneaux, V., Driouech, F., Adnani, M. E., Fazziki, A. E., Amenzou, N., Raibi, F., Mandour, A. E., Ibouh, H., Dantec, V. L., Habets, F., Tramblay, Y., Mougenot, B., Leblanc, M., Faïz, M. E., Drapeau, L., Coudert, B., Hagolle, O., Filali, N., Belaqziz, S., Marchane, A., Szczypta, C., Toumi, J., Diarra, A., Aouade, G., Hajhouji, Y., Nassah, H., Bigeard, G., Chirouze, J., Boukhari, K., Abourida, A., Richard, B., Fanise, P., Kasbani, M., Chakir, A., Zribi, M., Marah, H., Naimi, A., Mokssit, A., Kerr, Y., and Escadafal, R.: Remote Sensing of Water Resources in Semi-Arid Mediterranean Areas: the joint international laboratory TREMA, International Journal of Remote Sensing, 36, 4879–4917, https://doi.org/10.1080/01431161.2015.1093198, https://doi.org/10.1080/01431161.2015.1093198, 2015.

Jarvis, P.: The interpretation of the variations in leaf water potential and stomatal conductance found in canopies in the field, Philosophical Transactions of the Royal Society of London. B, Biological Sciences, 273, 593–610, 1976.

Jasechko, S., Sharp, Z. D., Gibson, J. J., Birks, S. J., Yi, Y., and Fawcett, P. J.: Terrestrial water fluxes dominated by transpiration., Nature, 496, 347–50, https://doi.org/10.1038/nature11983, http://www.ncbi.nlm.nih.gov/pubmed/23552893, 2013.

Kalma, J. D., McVicar, T. R., and McCabe, M. F.: Estimating Land Surface Evaporation: A Review of Methods Using Remotely Sensed Surface Temperature Data, Surveys in Geophysics, 29, 421–469, https://doi.org/10.1007/s10712-008-9037-z, http://www.springerlink.com/index/10.1007/s10712-008-9037-z, 2008.

Kustas, W., Li, F., Jackson, T., Prueger, J., MacPherson, J., and Wolde, M.: Effects of remote sensing pixel resolution on modeled energy flux variability of croplands in Iowa, Remote Sensing of Environment, 92, 535 – 547, https://doi.org/https://doi.org/10.1016/j.rse.2004.02.020, http://www.sciencedirect.com/science/article/pii/S003442570400183X, 2002 Soil Moisture Experiment (SMEX02), 2004.

Kustas, W. P. and Norman, J. M.: A two-source approach for estimating turbulent fluxes using multiple angle thermal infrared observations, Water Resources Research, 33, 1495–1508, http://www.agu.org/pubs/crossref/1997/97WR00704.shtml, 1997.

Kustas, W. P. and Norman, J. M.: Evaluation of soil and vegetation heat flux predictions using a simple two-source model with radiometric temperatures for partial canopy cover, Agricultural and Forest Meteorology, 94, 13–29, https://doi.org/10.1016/S0168-1923(99)00005-2, http://www.sciencedirect.com/science/article/pii/S0168192399000052http://linkinghub.elsevier.com/retrieve/pii/S0168192399000052, 1999.

Kustas, W. P. and Norman, J. M.: Evaluating the effects of subpixel heterogeneity on pixel average fluxes, Remote Sensing of Environment, 342, 327–342, http://www.sciencedirect.com/science/article/pii/S0034425799000814, 2000.

Kustas, W. P., Norman, J. M., Anderson, M. C., and French, A. N.: Estimating subpixel surface temperatures and energy fluxes from the vegetation index–radiometric temperature relationship, Remote Sensing of Environment, 85, 429 – 440, https://doi.org/https://doi.org/10.1016/S0034-4257(03)00036-1, http://www.sciencedirect.com/science/article/pii/S0034425703000361, 2003.

Kustas, W. P., Alfieri, J. G., Anderson, M. C., Colaizzi, P. D., Prueger, J. H., Evett, S. R., Neale, C. M., French, A. N., Hipps, L. E., Chávez, J. L., et al.: Evaluating the two-source energy balance model using local thermal and surface flux observations in a strongly advective irrigated agricultural area, Advances in Water Resources, 50, 120–133, 2012.

Lafleur, P. M. and Rouse, W. R.: Application of an energy combination model for evaporation from sparse canopies, Agricultural and Forest Meteorology, 49, 135 – 153, https://doi.org/https://doi.org/10.1016/0168-1923(90)90047-A, http://www.sciencedirect.com/science/article/pii/016819239090047A, 1990.

Lagouarde, J.-P., Bach, M., Sobrino, J. A., Boulet, G., Briottet, X., Cherchali, S., Coudert, B., Dadou, I., Dedieu, G., Gamet, P., Hagolle, O., Jacob, F., Nerry, F., Olioso, A., Ottlé, C., Roujean, J.-l., and Fargant, G.: The MISTIGRI thermal infrared project: scientific objectives

and mission specifications, International Journal of Remote Sensing, 34, 3437–3466, https://doi.org/10.1080/01431161.2012.716921, http://www.tandfonline.com/doi/abs/10.1080/01431161.2012.716921, 2013.

Li, F.: Deriving land surface temperature from Landsat 5 and 7 during SMEX02/SMACEX, Remote Sensing of Environment, 92, 521–534, https://doi.org/10.1016/j.rse.2004.02.018, http://linkinghub.elsevier.com/retrieve/pii/S0034425704001877, 2004.

Li, F. and Kustas, W. P.: Utility of remote sensing-based two-source energy balance model under low-and high-vegetation cover conditions, Journal of . . . , pp. 878–891, http://journals.ametsoc.org/doi/abs/10.1175/JHM464.1, 2005.

Li, F., Kustas, W. P., Anderson, M. C., Jackson, T. J., Bindlish, R., and Prueger, J. H.: Comparing the utility of microwave and thermal remote-sensing constraints in two-source energy balance modeling over an agricultural landscape, Remote Sensing of Environment, 101, 315–328, https://doi.org/10.1016/j.rse.2006.01.001, http://linkinghub.elsevier.com/retrieve/pii/S0034425706000253, 2006.

Li, F., Kustas, W. P., Anderson, M. C., Prueger, J. H., and Scott, R. L.: Effect of remote sensing spatial resolution on interpreting tower-based flux observations, Remote Sensing of Environment, 112, 337–349, https://doi.org/10.1016/j.rse.2006.11.032, http://linkinghub.elsevier.com/retrieve/pii/S0034425707003069, 2008.

Liu, Y., Hiyama, T., and Yamaguchi, Y.: Scaling of land surface temperature using satellite data: A case examination on ASTER and MODIS products over a heterogeneous terrain area, Remote Sensing of Environment, 105, 115–128, https://doi.org/10.1016/j.rse.2006.06.012, http://linkinghub.elsevier.com/retrieve/pii/S0034425706002379, 2006.

McCabe, M. F. and Wood, E. F.: Scale influences on the remote estimation of evapotranspiration using multiple satellite sensors, Remote Sensing of Environment, 105, 271–285, https://doi.org/10.1016/j.rse.2006.07.006, http://linkinghub.elsevier.com/retrieve/pii/S0034425706002586, 2006.

Milly, P. C. D.: Climate, soil water storage, and the average annual water balance, Water Resources Research, 30, 2143–2156, https://doi.org/10.1029/94WR00586, http://doi.wiley.com/10.1029/94WR00586, 1994.

Moncrieff, J. B., Massheder, J., de Bruin, H., Elbers, J., Friborg, T., Heusinkveld, B., Kabat, P., Scott, S., Soegaard, H., and Verhoef, A.: A system to measure surface fluxes of momentum, sensible heat, water vapour and carbon dioxide, Journal of Hydrology, 188-189, 589–611, http://www.sciencedirect.com/science/article/B6V6C-4D03X01-11/2/4e6869e1799144b149afc02a22cbcee3, 1997.

Monteith, J.: Evaporation and environment, Symp. Soc. Exp. Biol, http://www.unc.edu/courses/2007fall/geog/801/001/www/ET/Monteith65.pdf, 1965.

Mualem, Y.: A new model for predicting the hydraulic conductivity of unsaturated porous media, Water Resources Research, 12, 513–522, https://doi.org/10.1029/WR012i003p00513, http://onlinelibrary.wiley.com/doi/10.1029/WR012i003p00513/full, 1976.

Norman, Kustas, and Humes: Source approach for estimating soil and vegetation energy fluxes in observations of directional radiometric surface temperature, Agricultural and Forest Meteorology, 77, 263–293, https://doi.org/10.1016/0168-1923(95)02265-Y, http://linkinghub.elsevier.com/retrieve/pii/016819239502265Y, 1995.

Norman, J., Kustas, W., Prueger, J., and Diak, G.: Surface flux estimation using radiometric temperature: A dual-temperature-difference method to minimize measurement errors, Water Resources Research, 36, 2263–2274, 2000.

Norman, J. M., Anderson, M. C., Kustas, W. P., French, A. N., Mecikalski, J., Torn, R., Diak, G. R., Schmugge, T. J., and Tanner, B. C. W.: Remote sensing of surface energy fluxes at 101-m pixel resolutions, Water Resources Research, 39, n/a–n/a, https://doi.org/10.1029/2002WR001775, http://dx.doi.org/10.1029/2002WR001775, 1221, 2003.

Olioso, A., Chauki, H., Courault, D., and Wigneron, J.-P.: Estimation of Evapotranspiration and Photosynthesis by Assimilation of Remote Sensing Data into SVAT Models, Remote Sensing of Environment, 68, 341–356, https://doi.org/10.1016/S0034-4257(98)00121-7, http://linkinghub.elsevier.com/retrieve/pii/S0034425798001217, 1999.

Peres, L. F. and DaCamara, C. C.: Land surface temperature and emissivity estimation based on the two-temperature method: sensitivity analysis using simulated MSG/SEVIRI data, Remote Sensing of Environment, 91, 377–389, http://www.sciencedirect.com/science/article/B6V6V-4CBDFJD-1/2/d98f3af097368d8e98e37c6124733be9, 2004.

Petropoulos, G., Wooster, M., Carlson, T., Kennedy, M., and Scholze, M.: A global Bayesian sensitivity analysis of the 1d SimSphere soil–vegetation–atmospheric transfer (SVAT) model using Gaussian model emulation, Ecological Modelling, 220, 2427–2440, 2009.

Pitman, A., Henderson-Sellers, A., Desborough, C., Yang, Z.-L., Abramopoulos, F., Boone, A., Dickinson, R., Gedney, N., Koster, R., Kowalczyk, E., Lettenmaier, D. P., Liang, X., Mahfouf, J.-F., Noilhan, J., Polcher, J., Qu, W., Robock, A., Rosenzweig, C., Schlosser, C., Shmakin, A., Smith, J., Suarez, M., Verseghy, D., Wetzel, P., Wood, E. F., and Xue, Y.: Key results and implications from phase 1(c) of the Project for Intercomparison of Land-surface Parametrization Schemes, Climate Dynamics, 15, 673–684, https://doi.org/10.1007/s003820050309, http://www.springerlink.com/openurl.asp?genre=article&id=doi:10.1007/s003820050309, 1999.

Prevot, L., Bernard, R., Taconet, O., Vidal-Madjar, D., and Thony, J. L.: Evaporation From a Bare Soil Evaluated Using a Soil Water Transfer Model and Remotely Sensed Surface Soil Moisture Data, Water Resources Research, 20, 311–316, https://doi.org/10.1029/WR020i002p00311, http://dx.doi.org/10.1029/WR020i002p00311, 1984.

Priestley, C. H. B. and Taylor, R. J.: On the Assessment of Surface Heat Flux and Evaporation Using Large-Scale Parameters, Monthly Weather Review, 100, 81–92, https://doi.org/10.1175/1520-0493(1972)100<0081:OTAOSH>2.3.CO;2, 1972.

Quintana-Seguí, P., Le Moigne, P., Durand, Y., Martin, E., Habets, F., Baillon, M., Canellas, C., Franchisteguy, L., and Morel, S.: Analysis of Near-Surface Atmospheric Variables: Validation of the SAFRAN Analysis over France, Journal of Applied Meteorology and Climatology, 47, 92–107, https://doi.org/10.1175/2007JAMC1636.1, http://journals.ametsoc.org/doi/abs/10.1175/2007JAMC1636.1, 2008.

Ritter, B. and Geleyn, J.-F.: A Comprehensive Radiation Scheme for Numerical Weather Prediction Models with Potential Applications in Climate Simulations, Monthly Weather Review, 120, 303–325, https://doi.org/10.1175/1520-0493(1992)120<0303:ACRSFN>2.0.CO;2, http://journals.ametsoc.org/doi/abs/10.1175/1520-0493(1992)120<0303:ACRSFN>2.0.CO;2, 1992.

Robock, A., Luo, L., Wood, E. F., Wen, F., Mitchell, K. E., Houser, P. R., Schaake, J. C., Lohmann, D., Cosgrove, B., Sheffield, J., et al.: Evaluation of the North American Land Data Assimilation System over the southern Great Plains during the warm season, Journal of Geophysical Research: Atmospheres, 108, 2003.

Roos, J.: The radiation regime and architecture of plants, vol. 3, W. Junk, 1991.

Santanello, J., Joseph, A., and Friedl, M. A.: Diurnal covariation in soil heat flux and net radiation, Journal of Applied Meteorology, 42, 851–862, 2003.

Schmetz, J., Pili, P., Tjemkes, S., Just, D., Kerkmann, J., Rota, S., and Ratier, A.: Supplement to An Introduction to Meteosat Second Generation (MSG), Bulletin of the American Meteorological Society, 83, 991–991, https://doi.org/10.1175/BAMS-83-7-Schmetz-1, http://journals.ametsoc.org/doi/abs/10.1175/BAMS-83-7-Schmetz-1, 2002.

Sellers, P., Berry, J., Collatz, G., Field, C., and Hall, F.: Canopy reflectance, photosynthesis, and transpiration. III. A reanalysis using improved leaf models and a new canopy integration scheme., Remote Sensing of Environment, 42, 187–216, https://doi.org/10.1016/0034-4257(92)90102-P, http://www.sciencedirect.com/science/article/pii/003442579290102Phttp://linkinghub.elsevier.com/retrieve/pii/003442579290102P, 1992.

Sellers, P., Randall, D., and Collatz, G.: A revised land surface parameterization (SiB2) for atmospheric GCMs. Part I: Model formulation, Journal of . . . , http://journals.ametsoc.org/doi/abs/10.1175/1520-0442(1996)009%3C0676%3AARLSPF%3E2.0.CO%3B2, 1996.

Shukla, J. and Mintz, Y.: Influence of Land-Surface Evapotranspiration on the Earth's Climate, American Association for the Advancement of Science, 215, 1498–1501, https://doi.org/10.2307/1688150, http://www.jstor.org/stable/1688150, 1982.

Shuttleworth, W. J. and Wallace, J. S.: Evaporation from sparse crops-an energy combination theory, Quarterly Journal of the Royal Meteorological Society, 111, 839–855, https://doi.org/10.1002/qj.49711146910, http://doi.wiley.com/10.1002/qj.49711146910, 1985.

Soares, J., Bernard, R., Taconet, O., Vidal-Madjar, D., and Weill, A.: Estimation of bare soil evaporation from airborne measurements, Journal of Hydrology, 99, 281–296, https://doi.org/10.1016/0022-1694(88)90054-6, http://linkinghub.elsevier.com/retrieve/pii/0022169488900546, 1988.

Taylor, K. E.: Summarizing multiple aspects of model performance in a single diagram, Journal of Geophysical Research, 106, 7183, https://doi.org/10.1029/2000JD900719, http://www.agu.org/pubs/crossref/2001/2000JD900719.shtml, 2001.

Thom, A. S.: Momentum, mass and heat exchange of vegetation, Quarterly Journal of the Royal Meteorological Society, 98, 124–134, https://doi.org/10.1002/qj.49709841510, http://doi.wiley.com/10.1002/qj.49709841510, 1972.

Timmermans, W. J., Kustas, W. P., Anderson, M. C., and French, A. N.: An intercomparison of the Surface Energy Balance Algorithm for Land (SEBAL) and the Two-Source Energy Balance (TSEB) modeling schemes, Remote Sensing of Environment, 108, 369–384, https://doi.org/10.1016/j.rse.2006.11.028, http://linkinghub.elsevier.com/retrieve/pii/S0034425706005013, 2007.

Timmermans, W. J., Jimenez-Munoz, J.-C., Hidalgo, V., Richter, K., Sobrino, J. A., D'Urso, G., Satalino, G., Mattia, F., De Lathauwer, E., and Pauwels, V. R. N.: Estimation of the Spatially Distributed Surface Energy Budget for AgriSAR 2006, Part I: Remote Sensing Model Intercomparison, IEEE Journal of Selected Topics in Applied Earth Observations and Remote Sensing, 4, 465–481, https://doi.org/10.1109/JSTARS.2010.2098019, http://ieeexplore.ieee.org/xpls/abs_all.jsp?arnumber=5680923http://ieeexplore.ieee.org/lpdocs/epic03/wrapper.htm?arnumber=5680923, 2011.

Wan, Z.: New refinements and validation of the MODIS Land-Surface Temperature/Emissivity products, Remote Sensing of Environment, 112, 59–74, https://doi.org/10.1016/j.rse.2006.06.026, http://linkinghub.elsevier.com/retrieve/pii/S0034425707003665, 2008.

Wetzel, P. and Chang, J.-T.: Evapotranspiration from nonuniform surfaces: A first approach for short-term numerical weather prediction, Monthly weather review, 116, 600–621, http://cat.inist.fr/?aModele=afficheN&cpsidt=7827724, 1988.

Wilson, K., Goldstein, A., Falge, E., Aubinet, M., Baldocchi, D., Berbigier, P., Bernhofer, C., Ceulemans, R., Dolman, H., Field, C., Grelle, A., Ibrom, A., Law, B., Kowalski, A., Meyers, T. P., Moncrieff, J. B., Monson, R., Oechel, W., Tenhunen, J., Valentini, R., and Verma, S.: Energy balance closure at FLUXNET sites, Agricultural and Forest Meteorology, 113, 223–243, https://doi.org/10.1016/S0168-1923(02)00109-0, http://linkinghub.elsevier.com/retrieve/pii/S0168192302001090, 2002.

Wood, E. F., Lettenmaier, D. P., and Liang, X.: The Project for Intercomparison of Land-surface Parameterization Schemes (PILPS) Phase 2 (c) Red–Arkansas River basin experiment:: 1. Experiment description, Global and Planetary . . . , pp. 115–135, http://www.sciencedirect.com/science/article/pii/S0921818198000447, 1998.

Zhan, X., Kustas, W. P., and Humes, K.: An intercomparison study on models of sensible heat flux over partial canopy surfaces with remotely sensed surface temperature, Remote Sensing of Environment, 4257, http://www.sciencedirect.com/science/article/pii/S0034425796000491, 1996.

Table 3. Sites characteristics and overview of available cultures and crop cycles.

Site		**Auradé**	**Lamasquère**	**Sidi Rahal**
Location		France	France	Morocco
Latitude		43.54984444 °N	43.49737222 °N	31.665852 °N
Longitude		1.10563611 °E	1.23721944 °E	7.597873 °W
Climate		temperate	temperate	semi-arid
Soil type		Clay loam	Clay	Clay
sand[%] silt[%] clay[%]		21 47 32	12 34 54	20 34 46
Depth [m]		0.6	1	1
Slope [%]		2	0	1
2004	Culture	-	-	**Wheat ***
	Growth cycle length [$days$]	-	-	133
	Maximum LAI [$m^2\ m^{-2}$]	-	-	3.76
	Cumulated rain [mm]	-	-	135
	Cumulated irrigation [mm]	-	-	120
2006	Culture	**Wheat**	**Corn ***	-
	Growth cycle length [$days$]	246	123	-
	Maximum LAI [$m^2\ m^{-2}$]	3.13	3.33	-
	Cumulated rain [mm]	397	132	-
	Cumulated irrigation [mm]	0	148	-
2007	Culture	**Sunflower**	**Wheat**	-
	Growth cycle length [$days$]	157	271	-
	Maximum LAI [$m^2\ m^{-2}$]	1.74	4.47	-
	Cumulated rain [mm]	456	531	-
	Cumulated irrigation [mm]	0	0	-
2008	Culture	**Wheat**	**Corn ***	-
	Growth cycle length [$days$]	248	175	-
	Maximum LAI [$m^2\ m^{-2}$]	2.39	3.28	-
	Cumulated rain [mm]	491	397	-
	Cumulated irrigation [mm]	0	50	-

* irrigated cultures.

Table 4. Intercomparison of TSEB and SEtHyS performances (RMSE), with influence of time resolution, phenological stage, culture and climate.

		RMSE [$W\ m^{-2}$]					
		R_n		H		LE	
		TSEB	SEtHyS	TSEB	SEtHyS	TSEB	SEtHyS
Time resolution	Overall (time step)	46.5	25.7	28.9	38.0	54.7	47.1
	Overall (daily average)	42.7	18.9	21.2	28.7	38.9	35.5
Phenology	Rising	22.1	15.3	110.2	44.1	88.3	44.0
	Growth	30.9	24.5	21.7	28.3	51.6	43.4
	Max of vegetation	51.1	20.2	24.6	40.8	55.5	48.1
	Senescence	55.0	29.4	43.5	47.3	54.0	42.1
	Hydric stress	53.2	21.6	44.9	49.3	49.6	30.6
Culture	Wheat	49.7	29.5	32.9	37.6	49.2	45.6
	Corn	46.0	18.1	22.9	40.2	64.4	52.6
	Sunflower	39.1	27.2	27.1	35.1	49.0	39.5
Climate	France (wheat)	35.1	32.6	35.1	36.4	52.5	42.9
	Morocco (wheat)	25.6	15.2	25.6	40.8	36.3	53.4

Table 5. Comparison of *in situ* data and spatial data (SAFRAN, ASTER, and inversed NDVI)

Forcing	**Source**	**Variables [unit]**	**Description**	**Mean error**		**"Extreme" error**	
				RMSE	BIAS	1^{st} decile	9^{th} decile
Meteo	SAFRAN	T_a $[°C]$	Air temperature	1.5	0.7	-1.5 (-10 %)	1.3 (+10 %)
		U_a $[m\ s^{-1}]$	Wind speed	1.4	-0.7	-0.65 (-30 %)	2.3 (+90 %)
		R_h $[\%]$	Relative humidity	7	8	-12 (-15 %)	5(+8 %)
		R_g $[W\ m^{-2}]$	Global radiation	90	35	-186 (-40 %)	125 (+60 %)
		R_a $[W\ m^{-2}]$	Atmospheric radiation	30	14	-51 (-15 %)	20 (+7 %)
Vegetation	FORMOSAT	LAI $[m^2\ m^{-2}]$	Leaf Area Index	-	20 %	-50 %	+50 %
		h_c $[m]$	Canopy height	-	20 %	-100 %	+100 %
LST	ASTER	T_s $[K]$	Surface temperature	2	-	-	-